NASA TECHNICAL MEMORANDUM

NASA TM X-64833

CMG-INDUCED LST DYNAMICS

By Sherman M. Seltzer
Astrionics Laboratory

February 21, 1974

NASA

George C. Marshall Space Flight Center
Marshall Space Flight Center, Alabama

ACKNOWLEDGMENT

I wish to gratefully acknowledge the contributions and efforts of Mr. Paul H. Fisher, Guidance and Control Systems Branch, Astrionics Laboratory, MSFC in the simulation of the analytically derived results. I further wish to acknowledge the thorough and diligent efforts of Mr. Hans H. Hosenthien, Chief of the R&D Analysis Office, Astrionics Laboratory, in proof-reading this memorandum.

TABLE OF CONTENTS

LIST OF ILLUSTRATIONS

LIST OF ILLUSTRATIONS (Continued)

LIST OF ILLUSTRATIONS (Concluded)

LIST OF TABLES

NOMENCLATURE

A	limit cycle amplitude
A_0, A_1	vehicle attitude control gains for Dahl model
$\bar{A}$, $\bar{B}$	weighted vehicle control gains for Bendix model number 1, Case I
$\bar{A}_1$, $\bar{B}_1$	numerator of N_1 and N_2, respectively
a	$\equiv 2\gamma A T_{GFo}$
D	dead zone
$f(x)$	assumed sinusoidal output of nonlinearity N
$G(s)$	general form for transfer function representing linear portion of overall plant
$G_G(s)$	general form for transfer function representing linear portion of CMG
H	angular momentum
I_{GE}	CMG gimbal effective moment of inertia
I_v	vehicle moment of inertia
J	Jacobian
K_0, K_1	weighted vehicle control gains for Bendix model number 1, Sperry model, and Dahl model
$\bar{K}_0$, $\bar{K}_1$	weighted vehicle control gains for Bendix model number 1, Case III
K_I, K_p	CMG gimbal rate control gains for Dahl model

NOMENCLATURE (Continued)

K_G, g_0, g_1	characteristic parameters of second order model of CMG
k	primary slope of Bendix model number 1 nonlinearity
k_0, k_1	weighted vehicle control gains for Bendix model number 1, Case II
k_F	CMG feedback gain for Sperry model
k_T, k_γ	multiplication factors associated with T_{GFo} and γ, respectively
M	relay gain
m	secondary slope of Bendix model number 1 nonlinearity
N	nonlinear gain, characterized herein as a describing function
N_1	real part of Dahl model describing function
N_2	imaginary part of Dahl model describing function
R(s)	attitude rate sensor transfer function
s	complex variable (Laplace operator)
T_c	torque command to vehicle
T_f	CMG output gimbal pivot frictional torque
T_{GFo}	running friction torque
T_o	torque response of vehicle
	time

NOMENCLATURE (Continued)

u	$\equiv D/A$
x	sinusoidal input to nonlinearity N
y	$\equiv \frac{d T_f}{d \theta}$
ln	natural logarithm
ℓ	$\equiv 2a^2 + 2a + 1$
Ω	imaginary part of s associated with system frequency; as used herein, also limit cycle frequency of oscillation
α, β	weighted vehicle control gains for Bendix model number 1, Case IV
γ	CMG gimbal pivot friction parameter
δ	CMG output gimbal angle
$\dot{\delta}$	CMG output gimbal angle rate
$\dot{\delta}_c$	commanded CMG output gimbal angle rate
ζ_{CMG}	damping ratio of CMG
θ	vehicle attitude
κ_0, κ_1	CMG control gains for Sperry model
ξ	$\equiv Dk/M$
σ	$\equiv \gamma T^2_{GFo}$
ϕ	phase shift from x to f(x)

NOMENCLATURE (Concluded)

χ	commanded vehicle attitude
ω	imaginary component of s (identified with frequency)
ω_c	bandwidth of first order model of CMG
ω_g	bandwidth of first order model of attitude rate sensor
$\omega_n]_{CMG}$	natural frequency of CMG
$\dot{}$	derivative with respect to time

TECHNICAL MEMORANDUM X-64833

CMG-INDUCED LST DYNAMICS

INTRODUCTION

The nature of the control moment gyroscope (CMG) output gimbal bearing friction has been the subject of many discussions and presentations by various investigators. It is important to know the precise nature of the torque caused by the bearing friction so that its effect on the dynamic behavior of the Large Space Telescope (LST) and its pointing and control system (PCS) can be predicted. The objective of the analysis and supporting computer simulations reported herein is to study the effect of the assumed CMG nonlinearity upon the system dynamics in order to develop an understanding of the nature and effect of variations of numerical values of parameters upon the system. The weakness of the mathematical analysis used results from the need to restrict the complexity of the model studied; however, the design insight obtained is valuable.

The parameter plane analysis technique used herein makes use of the describing function to portray the nonlinearity representing CMG gimbal bearing friction. Where the describing function is a complex value, the technique developed for a system containing two nonlinearities may be applied [1]. This technique affords both analytic and graphic portrayal of the effects of variations in selected system parameters. With few exceptions (noted herein) the results are confirmed with analogue computer simulation.

Finally, the reader is cautioned against relying solely on computer simulations without adequate mathematical analysis as a background. An attempt to use an analogue computer to define stability boundaries for satellite dynamics as characterized by the Mathieu equation should convince even the skeptic of the weakness of computer simulation when not augmented by mathematical analysis. A current example in the field of digital simulation is the errors contained in Connell's paper [2] reported by Schiehlen [3].

The following four models are considered in this report; three of them are analyzed in detail.

1. A model developed by the Bendix Corporation and presented to MSFC in April 1972 [4-6][1,2]. A single axis representation of the CMG, rate gyro, and rigid body dynamics is shown in Figure 1.

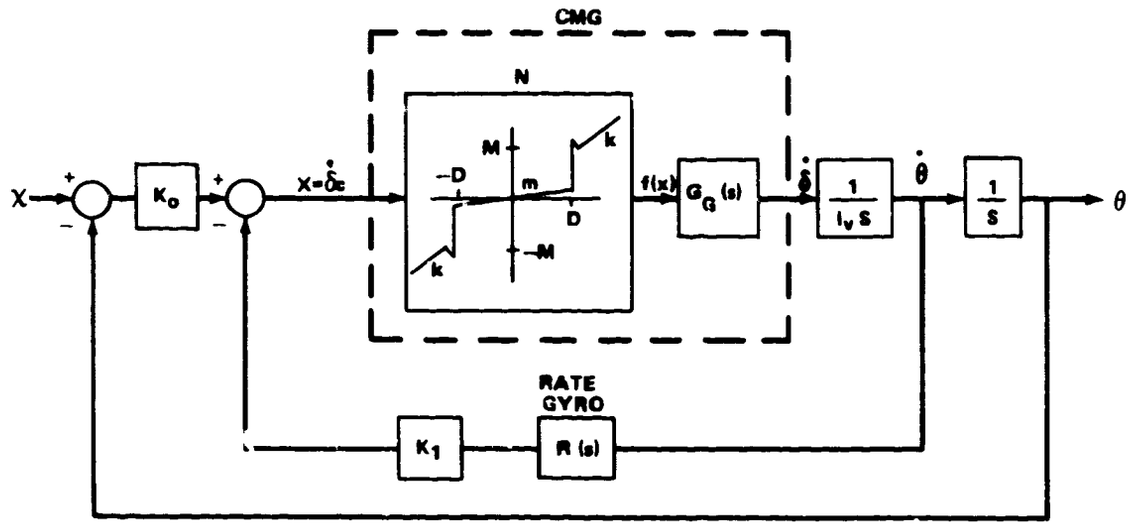

Figure 1. Bendix model number 1.

2. A Sperry model (Fig. 2) presented to MSFC in December 1972.

3. Another Bendix model presented in March 1973 (Fig. 3).

4. The model developed by Dr. P. R. Dahl of Aerospace Corporation (the so-called Dahl model). This model may be incorporated in a single axis representation (Fig. 4), where the nonlinear relation between the frictional torque (T_f) about the CMG output gimbal pivot and the gimbal rotation (δ) is portrayed as the nonlinearity N. The mathematical description, developed by Dahl, of this relation is

$$\dot{T}_f = y\dot{\delta} \quad , \tag{1}$$

1. CMG Considerations for HEAO and High Accuracy Point Missions. Written Presentation Material, Bendix Corp. Teterboro, N.J., April 21, 1972.

2. Whitley, G.W.: LST Fine Pointing Control System Design. MSFC S&E-ASTR-SD-78-72 Letter, Oct. 3, 1972.

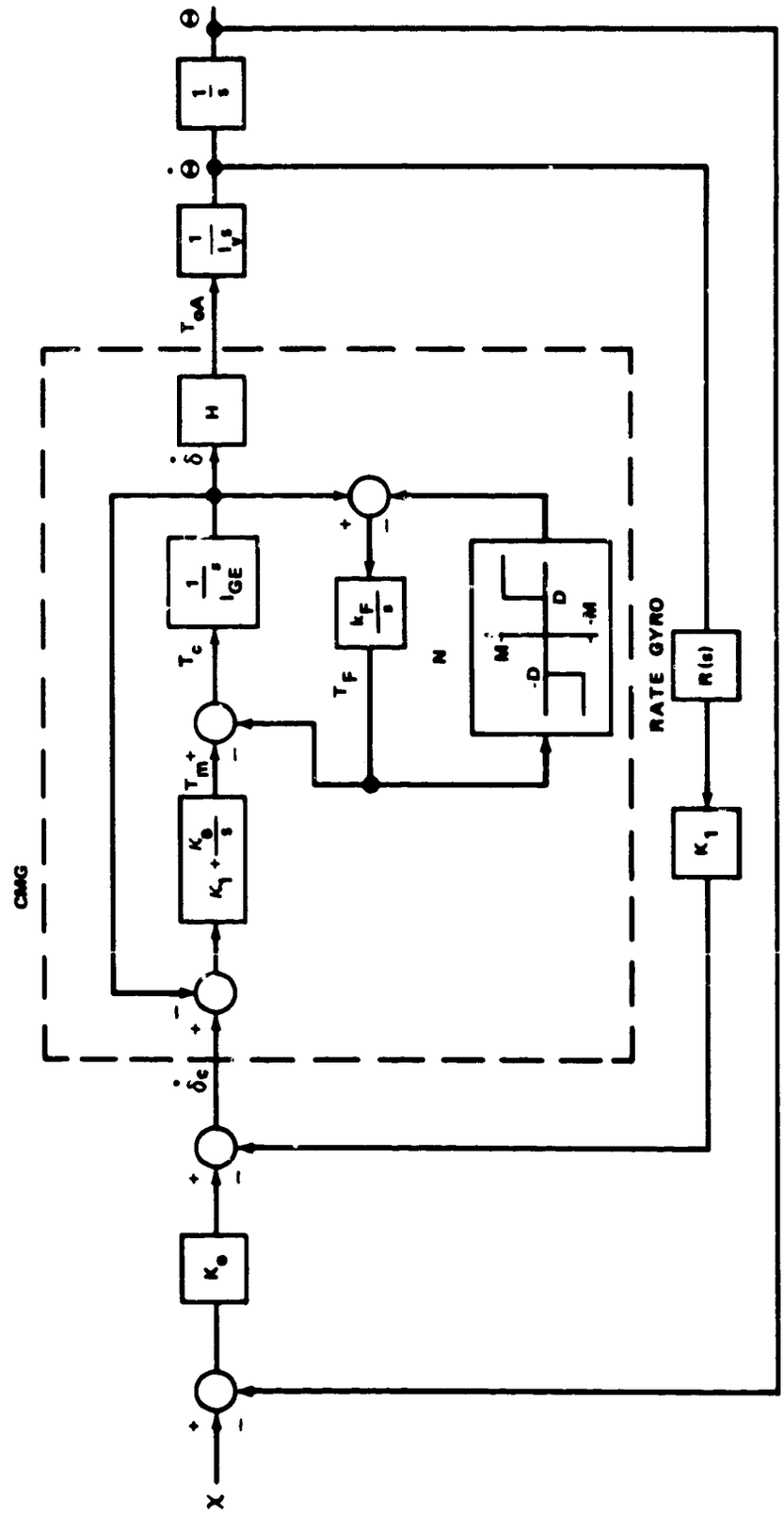

Figure 2. Sperry model.

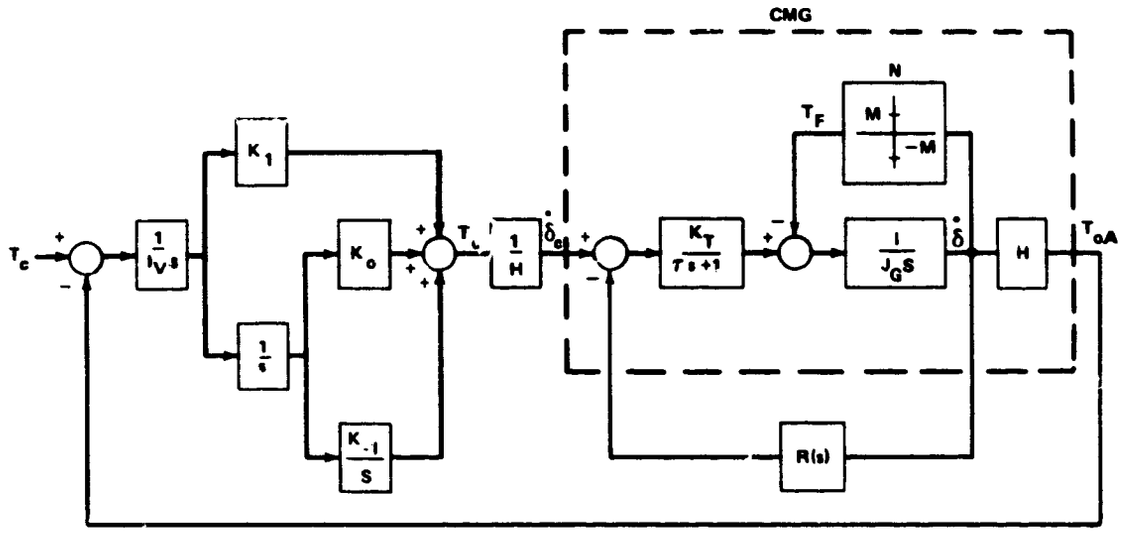

Figure 3. Bendix model number 2.

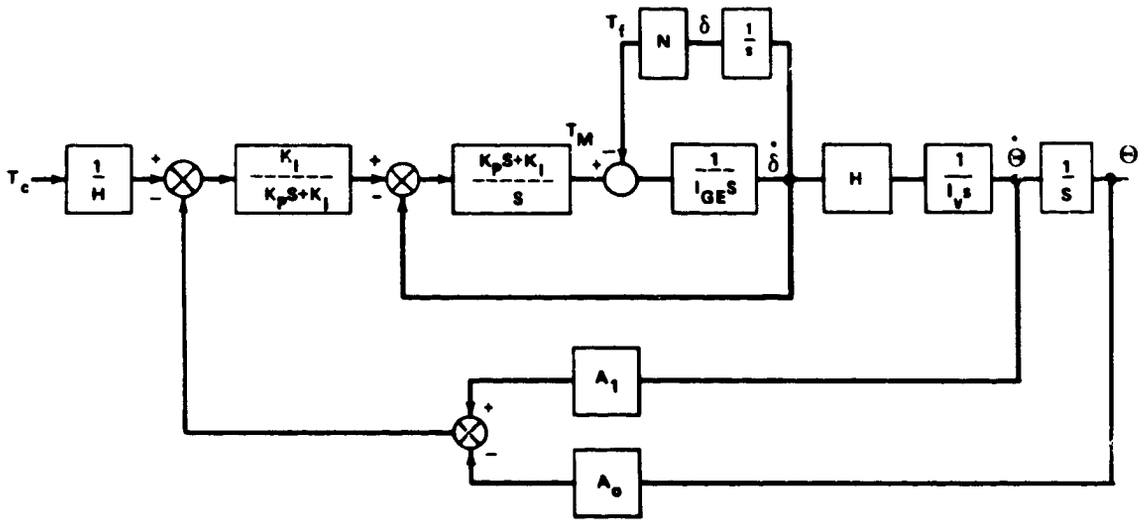

Figure 4. Single-axis model.

where

$$y \equiv \frac{dT_f}{d\delta} = \gamma(T_f \operatorname{sgn} \dot{\delta} - T_{GFo})^2 \qquad (2)$$

and is shown in Figure 5, where γ and T_{GFo} are parameters describing the friction relationship and the overdot represents differentiation with respect to time.

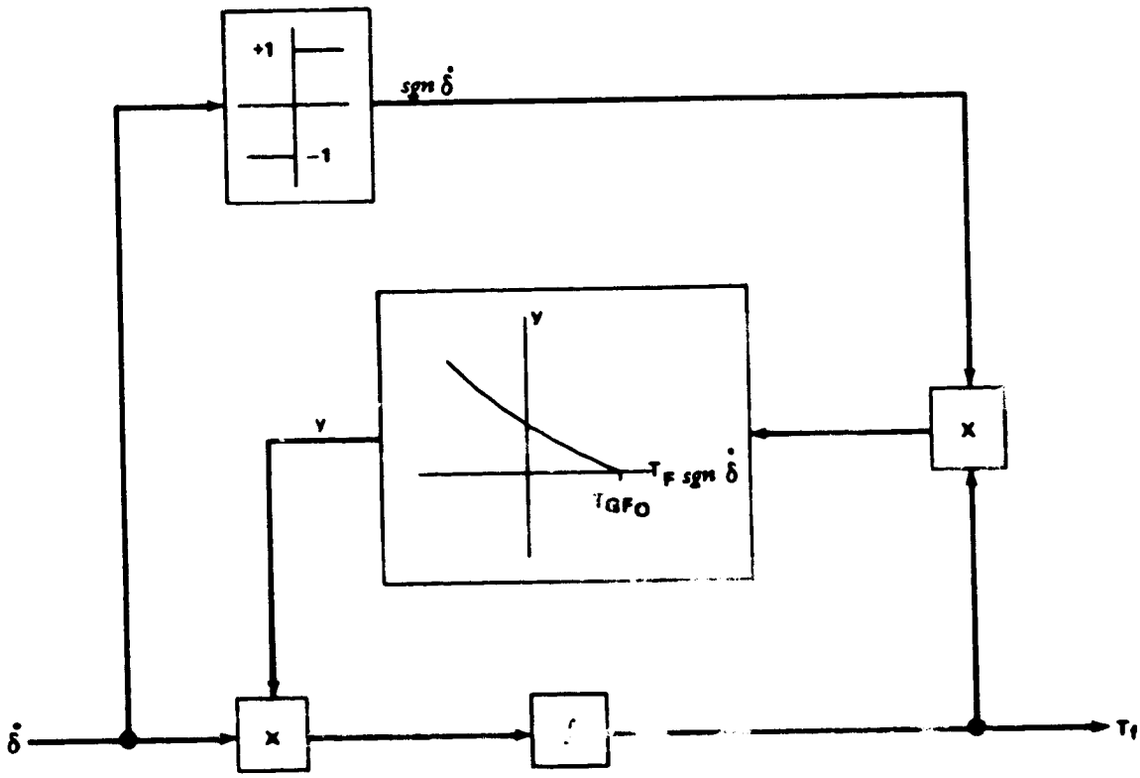

Figure 5. CMG friction nonlinearity a la Dahl.

ANALYSIS TECHNIQUE

The objective of the analyses presented herein is to determine stability conditions for systems that may be represented schematically, as in Figure 6. The plant under consideration is represented by a linear part G(s) and a nonlinear element N. In the sequel N will be used to represent the nonlinear friction characteristics of the CMG gimbal pivot. In particular it is of interest to investigate the possibility of existence of limit cycles and to determine their characteristics. As used herein the term "limit cycle" will be used synonomously with the term "self-excited sustained oscillation." Hence, a limit

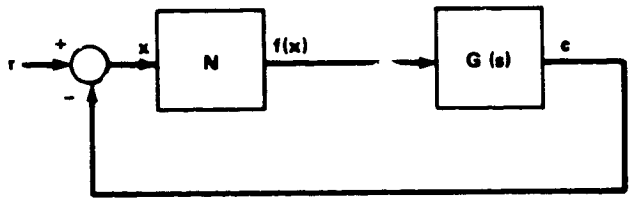

Figure 6. Basic nonlinear system.

cycle represents a steady-state oscillation to which or from which all neighboring trajectories in a state space will converge or diverge [7,8]. The stability of limit cycles may be defined in terms of three classes:

1. Stable (Orbitally Stable) Limit Cycle — If all neighboring state space trajectories converge to the limit cycle.

2. Unstable (Orbitally Unstable) Limit Cycle — If all neighboring state space trajectories diverge from the limit cycle.

3. Semistable (Orbitally Semistable) Limit Cycle — If state-space trajectories originating at points outside the limit cycle converge to it and those originating from points inside the limit cycle diverge from it, or vice versa.

Because of the low pass nature of the linear parts of the system plants under consideration, they are particularly amenable to analysis through application of describing function theory. Hence a detailed discussion of appropriate describing functions is needed [9]. It is assumed that, if a sustained oscillation occurs, the input x is described by

$$x = A \sin \Omega t \quad . \tag{3}$$

It is assumed that the output f(x) is approximated by the relation

$$f(x) \approx NA \sin (\Omega + \phi)t \quad , \tag{4}$$

where ϕ represents a phase shift.

The method of analysis used is defined in Reference 1 and embodies a describing function technique developed by Siljak [10]. It is assumed that the system being analyzed is amenable to describing function analysis and the system parameters are time-invariant. In essence, a describing function (N) is used to represent the nonlinearity. The characteristic equation representing the system is then obtained. For a limit cycle to occur, it is required that all characteristic equation roots have negative real parts except for one pair of roots which must be purely imaginary roots. This condition is determined mathematically and for ease of visualization may be portrayed graphically. In the latter case, two adjustable parameters are selected, at least one of which must also contain N. (If N is a complex quantity, its real and imaginary components may be used as the two parameters and Reference 1 may be applied directly.) A correlation between these parameters and the roots of the characteristic equation is then determined by mapping stability contours from the complex s-plane onto the chosen parameter plane. For the systems considered herein, only three (and sometimes fewer) such stability boundaries exist and they are easily found.

The first boundary (the one associated with real roots of the characteristic equation) is found by setting $s = 0$ in the characteristic equation. (Graphically this boundary may be identified by single hachures.) The second one (the one associated with purely imaginary roots) is found by setting $s = i\omega$. (This boundary is identified by cross-hachures.) The third one, called the boundary at infinity (in topological mapping from the complex s-plane to the Riemann sphere, it is associated with the sphere's north pole), is found by setting $1/s = 0$ in the characteristic equation. It also is identified by single hachures. From these boundaries, the stable region (if it exists) may be determined in terms of the selected adjustable parameters, for they bound the stable region.

The nonlinear locus of N as a function of the two adjustable parameters is determined next. The simultaneous solution of the nonlinear locus relation and the purely imaginary root boundary yields the condition for a limit cycle, assuming the indicated solution occurs adjacent to a stable region (which may not always be the case). This is readily apparent on the parameter plane as the intersection between the purely imaginary root boundary and the nonlinear locus. From this point of intersection, the frequency (identified as $\omega = \Omega$) and magnitude (A) of an indicated limit cycle may be determined as a function of the characteristics of the nonlinearity and of the adjustable parameters. Further, the behavior of the limit cycle when a small perturbation is applied to its amplitude, and, hence, the nature of limit cycle stability, also is apparent on the parameter plane.

ANALYSIS OF BENDIX MODEL NUMBER 1 (Fig. 1)

Four variations of Bendix model number 1 were studied and are identified herein as Cases I through IV:

1. Case I — This model consists of a perfect attitude rate sensor characterized by

$$R(s) = 1 \tag{5}$$

and a CMG characterized by the nonlinear element N and a first order transfer function

$$G_G(s) = \frac{\omega_c}{s + \omega_c} \quad . \tag{6}$$

This is the basic model considered.

2. Case II — A model characterized by a perfect attitude rate sensor, equation (5), and a CMG modeled as a nonlinear element N and a second order transfer function

$$G_G(s) = \frac{K_G}{s^2 + g_1 s + g_0} \quad . \tag{7}$$

The effect of a higher order model of the CMG is induced by comparing the results of the analyses of Cases I and II. It is similar to several models contained in the documents cited in References 4 and 5 and footnote 2.

3. Case III — A model consisting of an imperfect attitude rate sensor described by a first order transfer function

$$R(s) = \frac{\omega_g}{s + \omega_g} \tag{8}$$

and a first order characterization of the linear portion of the CMG, equation (6). This model permits an analysis of the effect of a nonperfect attitude rate sensor. It is the model documented in Reference 6 and footnote 2.

4. Case IV — An imperfect attitude rate sensor, equation (8), and a second order characterization of the linear portion of the CMG, equation (7). This model is similar to several models documented in References 4 and 5.

Because the precise nature of the relationship between the input (x) to the nonlinear element (N) of the CMG model and the output f(x) is obscure, the effect of variations of the parameters describing that relationship is studied. In particular it is desired to predict whether or not sustained oscillations in the vehicle's attitude and attitude rate will occur and, if so, what their characteristics are (in terms of amplitude, period, and stability) under various prescribed conditions.

Basic Nonlinearity

If the small overshoots occurring at $x = D$ and $x = -D$ (Fig. 1) are ignored, the describing function is

$$\frac{N}{k} = 1 - \frac{2}{\pi}\left[\left(1 - \frac{m}{k}\right)\sin^{-1}u + \left(1 - \frac{2}{\xi} - \frac{m}{k}\right)u\sqrt{1-u^2}\right], \quad u < 1 \tag{9a}$$

$$= m, \quad u > 1 \quad . \tag{9b}$$

For small values of m ($m << k$), the relation approximated by the describing function defined in equations (9) then becomes

$$\frac{N}{k} = 1 - \frac{2}{\pi}\left[\sin^{-1}u + \left(1 - \frac{2}{\xi}\right)u\sqrt{1-u^2}\right], \quad u \leq 1 \tag{10a}$$

$$= 0, \quad u > 1 \tag{10b}$$

where

$$u \stackrel{d.}{=} \frac{D}{A} \quad , \tag{10c}$$

and

$$\xi \stackrel{d.}{=} \frac{Dk}{M} \quad . \tag{10d}$$

Although the describing function may be found in a number of texts on nonlinear oscillations, this author was unable to locate a sketch of the variation of the describing function N with variations in the parameters A, D, M, and k. By selecting combinations of these parameters in a certain way, an interesting analogy between this particular describing function and a system familiar to control system engineers was discovered. Symbols D, M, and k are described on Figure 1; D represents the dead zone, and M and slope k characterize the gain through N. If N/k is plotted versus A/D with ξ as an independent parameter (Fig. 7), it is observed that all curves begin from a common point at N/k = 0 for A/D = 1 and asymptotically approach a value of unity for large values of A/D. If $\xi \geq 1$ the curves never rise above the value of unity. However, if $\xi < 1$ the curves rise from their initial value of zero to a peak value greater than unity and then (as A/D increases) approach the unity asymptote from above. The analogy to a second order control system is interesting. Here, ξ is analogous to the damping ratio ζ. Further study of the describing function reveals the amplitude of the peak value of N/k and the values of ξ and u (and hence D, M, and k) for which the peak occurs. If equation (10a) is optimized with respect to u, it is found that the peak value, N_0 k, of N/k occurs when u has the value

$$u_0 = \sqrt{\frac{\xi - 1}{\xi - 2}} \quad . \tag{11}$$

General (i.e., independent of numerical values for A, D, and k) curves of N_0/k versus ξ and A_0/D ($1/u_0$) versus ξ may be plotted from equations (10a) and (11) and are shown in Figure 8. These relationships will be used in subsequent predictions of limit cycle conditions.

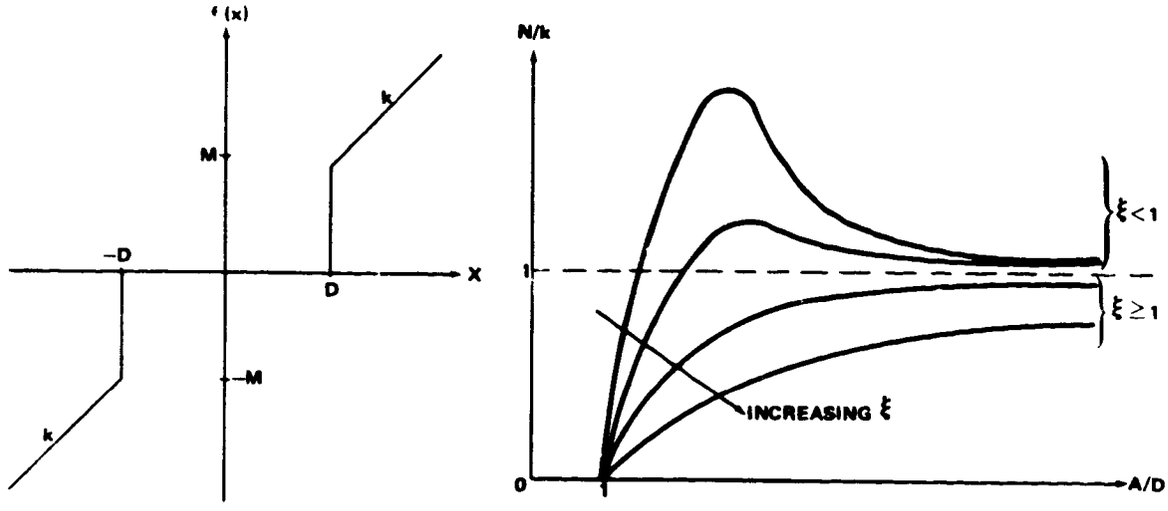

Figure 7. Describing functions for Bendix model number 1 nonlinearity (simplified).

Additional insight into the nature and dynamic effect of the nonlinearity's parameters A, D, and k may be obtained by considering certain limit cases.

Limit Case 1 (Ideal Relay). If the dead zone (D) of the basic nonlinearity (Fig. 1) is neglected and slope k decreased to zero, an ideal relay characteristic is obtained where

$$N = \frac{4M}{\pi A} \quad . \tag{12}$$

A diagram of this relationship is shown in Figure 9, setting $k = 0$.

Limit Case 2 (Relay With Dead Zone). If the dead zone of the basic nonlinearity is retained but slope k set at zero, a relay with dead zone characteristic is obtained where

$$N = \frac{4M\sqrt{1 - u^2}}{\pi A} \quad , \quad u \leq 1 \quad . \tag{13}$$

This relationship is shown in Figure 10. Observe that DN/M has a peak value. This may be found by setting $\xi = 0$ (since $k = 0$) in equation (11) and substituting $u_0 = D/A = 1/\sqrt{2}$ in equation (12) yielding a peak value of $DN/M = 2/\pi \approx 0.6366$.

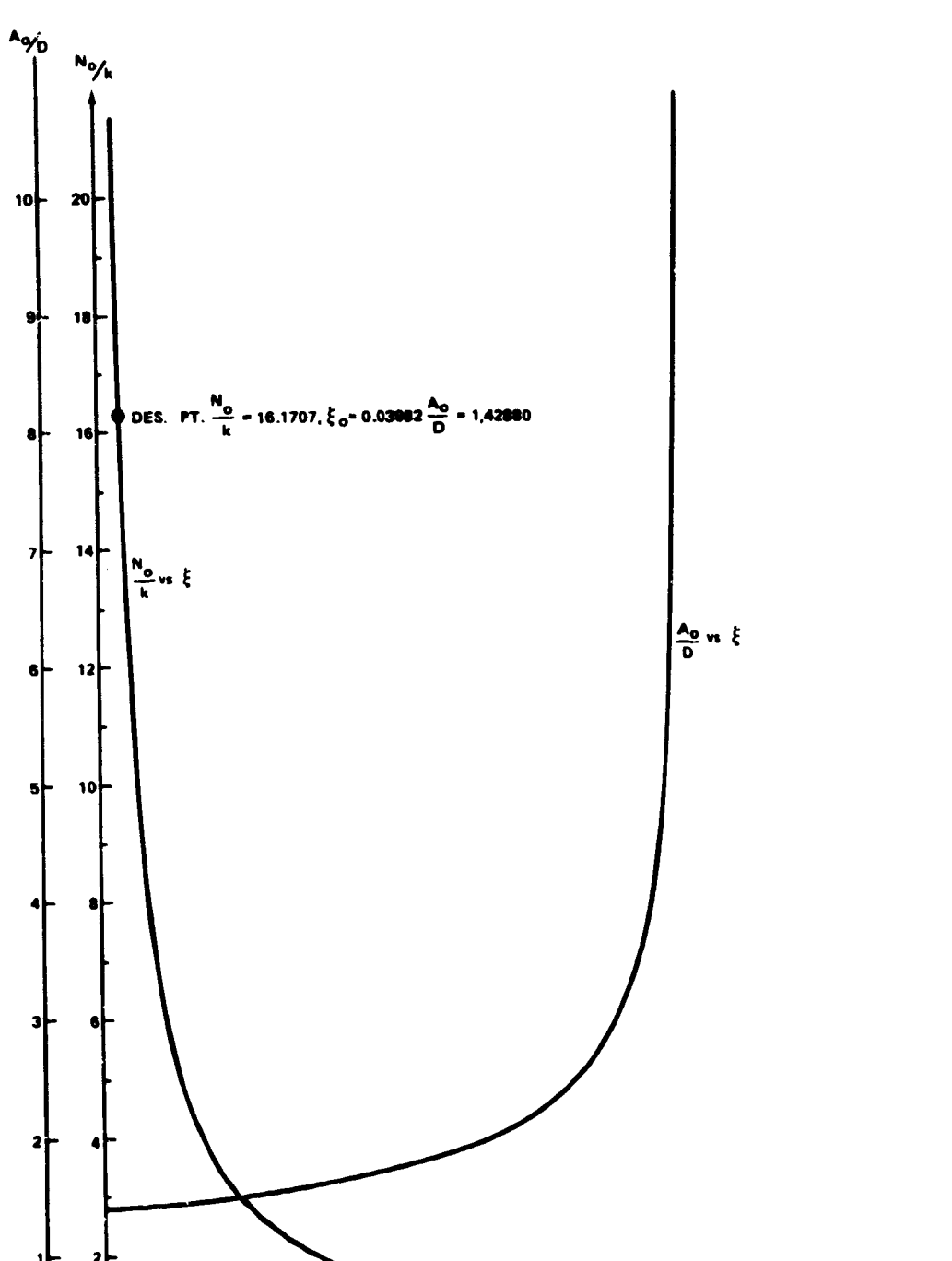

Figure 8. Peak value parameters of Bendix model number 1 nonlinearity (simplified).

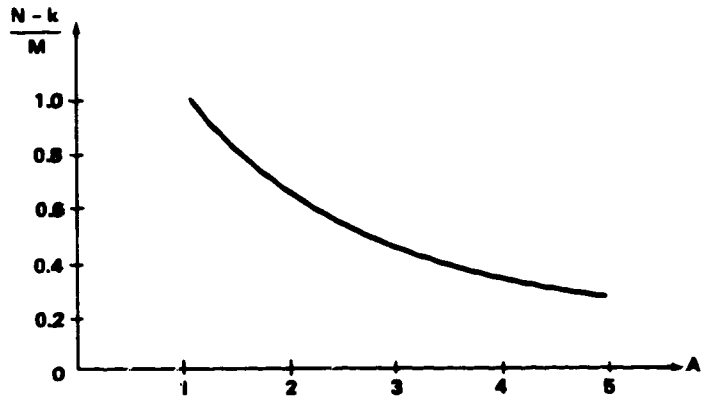

Figure 9. Describing function relation for ideal relay (k = 0) and preload (k > 0).

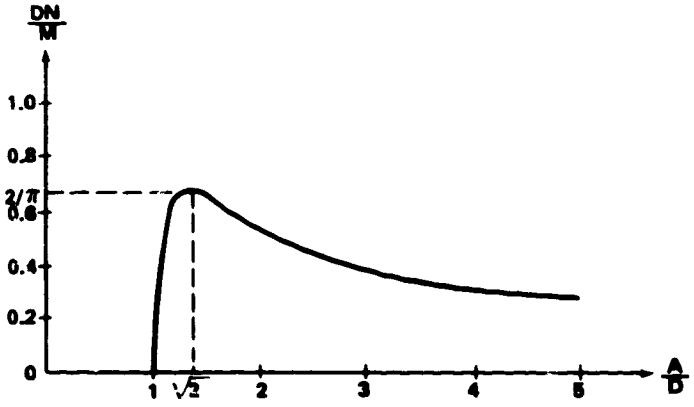

Figure 10. Describing function relation for relay with dead zone.

Limit Case 3 (Gain with Dead Zone). If the height M of the basic nonlinearity is collapsed to zero, a gain with dead zone characteristic results where

$$\frac{N}{k} = 1 - \frac{2}{\pi}\left(\sin^{-1} u + u\sqrt{1 - u^2}\right) \quad , \; u \leq 1 \quad . \tag{14}$$

This relationship is shown in Figure 11.

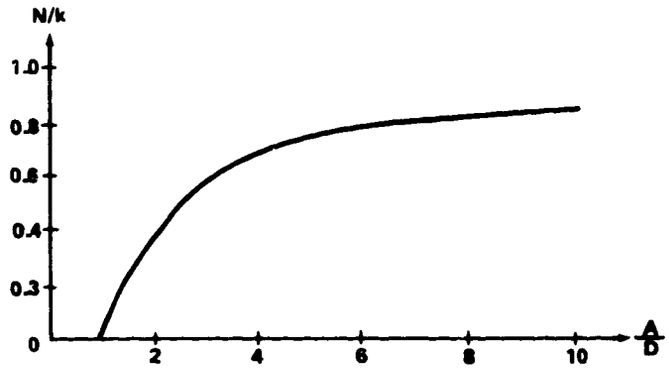

Figure 11. Describing function relation for gain with dead zone.

Limit Case 4 (Preload). If the dead zone of the basic nonlinearity is collapsed to zero, a preload characteristic results, yielding

$$\frac{N}{k} = \frac{4u}{\pi\xi} + 1 \quad . \tag{15}$$

This relationship is shown in Figure 9 with $k \neq 0$.

Limit Case 5 (Gain Change). If the parameter of M of the general nonlinearity (Fig. 1) is set equal to zero, a gain change characteristic results, yielding

$$\frac{N}{k} = 1 - \frac{2}{\pi}\left(1 - \frac{m}{k}\right)\left(\sin^{-1} u + u\sqrt{1-u^2}\right) \quad , \quad u \leq 1 \ , \tag{16}$$
$$= 1 \ , \quad u \geq 1 \ .$$

The relation is shown in Figure 12.

The four cases will now be analyzed in detail, considering the above limit cases [equations (12) through (16)] and the general case modified by setting m equal to zero [equations (10)].

Analysis of Case I

The characteristic equation is

$$s^3 + \omega_c s^2 + \overline{B}Ns + \overline{A}N = 0 \quad , \tag{17}$$

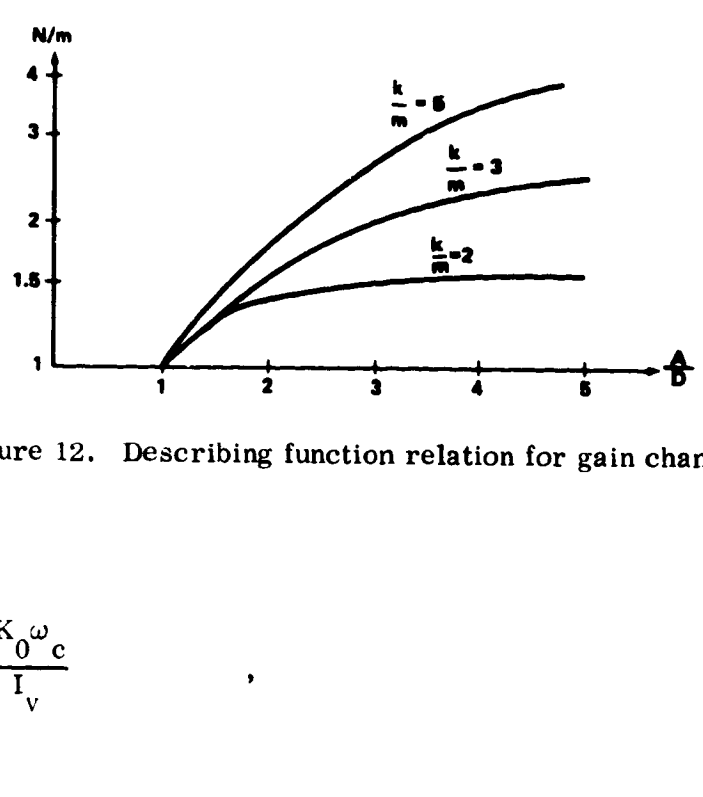

Figure 12. Describing function relation for gain change.

where

$$\bar{A} \triangleq \frac{K_0 \omega_c}{I_v} \quad , \tag{18a}$$

and

$$\bar{B} \triangleq \frac{K_1 \omega_c}{I_v} \quad . \tag{18b}$$

It is readily shown that the stable region of operation, in terms of parameters $\bar{A}N$, $\bar{B}N$ lies in the first quadrant and is bounded by the real root boundary ($\bar{A}N = 0$) and the imaginary root contour

$$\bar{B}N = \frac{\bar{A}N}{\omega_c} \quad . \tag{19}$$

From definitions (18), the nonlinear locus is seen to be a straight line through the origin with slope K_1/K_0. These two lines are shown on Figure 13. Since they cannot intersect, limit cycle operation is not indicated. A stable response is indicated if $K_1/K_0 > 1/\omega_c$ and, if $K_1/K_0 < 1/\omega_c$, the system response will be unstable.

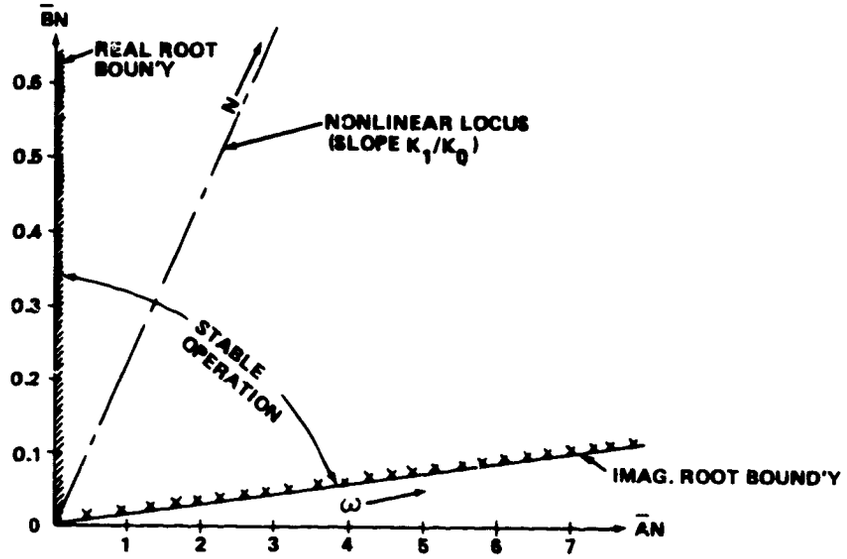

Figure 13. Case I (Bendix model number 1) — stability characteristics.

If the pitch axis is chosen as the single-axis about which rotational dynamics will be studied, the numerical values given in Table 1 may be used as representatives of the LST. With the exception of ω_c and ω_g, these values were obtained from Reference 5. The value for ω_c is obtained by matching the break frequency ω_c [equation (6)] with the break frequency of the second order system:

$$\omega_c = \sqrt{g_0/2} = 70.7 \text{ rad/s} \quad . \tag{20}$$

The value selected for ω_c is representative of a bandwidth-limited rate gyroscope and is low enough to indicate the dynamic effect of this degradation. Using Table 1 values, it is seen that a stable response is indicated, i.e., $K_1/K_0 > 1/\omega_c$.

Analysis of Case II

The characteristic equation is

$$s^4 + g_1 s^3 + g_0 s^2 + k_1 Ns + k_0 N = 0 \tag{21}$$

TABLE 1. LST NUMERICAL VALUES

Parameter	Numerical Value
g_0	$= K_G = 10^4$ (rad/s)^2
g_1	141.4 rad/s
H	610 Nms
I_{GE}	5.012 Nms^2 (3.7 ft lb s^2)
I_v	1.356×10^5 Nms^2
K_0	4.6843×10^6 Nm
K_1	1.1153×10^6 Nms
k_F	6.600×10^3 Nm/rad
ζ_{CMG}	0.707
κ_0	4.352×10^4 ($= \omega_n^2 I_G - b_f$)
κ_1	7.087×10^4 ($= 2 \zeta \omega_n I_G$)
ω_c	70.7 rad/s
ω_g	30 rad/s
$\omega_{n]CMG}$	100 rad/s

where

$$k_0 \stackrel{d.}{=} K_0 K_G / I_v \quad , \tag{22a}$$

and

$$k_1 \stackrel{d.}{=} K_1 K_G / I_v \quad . \tag{22b}$$

The real root boundary is

$$k_0 N = 0 \tag{23}$$

and the imaginary root boundary, in terms of parameters $k_0 N$ and $k_1 N$, may be written as

$$k_0 N = \frac{k_1 N \left(g_0 - \frac{k_1 N}{g_1} \right)}{g_1} \tag{24}$$

or, written as a function of the independent argument, frequency (ω),

$$k_0 N = \omega^2 (g_0 - \omega^2) \quad , \tag{25a}$$

$$k_1 N = g_1 \omega^2 \quad . \tag{25b}$$

From equations (22), the N-locus is expressed as

$$k_1 N = \left(\frac{K_1}{K_0}\right) k_0 N \quad . \tag{26}$$

A limit cycle and its characteristics are indicated by the simultaneous solution of equations (25) and (26), yielding

$$N = \frac{g_1 I_v}{K_1 K_G} \left(g_0 - \frac{K_0 g_1}{K_1}\right) \tag{27}$$

and

$$\Omega = \sqrt{g_0 - \frac{K_0 g_1}{K_1}} \quad . \tag{28}$$

The frequency Ω of the indicated limit cycle is determined by system parameters g_0, g_1, K_0, K_1 and has the same value regardless of the type of nonlinearity chosen for N. Although the value of N is also independent of the type of nonlinearity, the amplitude A of the limit cycle is dependent on the relation between N and A, e.g., equations (10), and (12) through (16). Equations (23), (25), and (26), are plotted on Figure 14. The simultaneous solution of equations (25) and (26) is indicated by the intersection labeled limit cycle.

Before numerical values are used, some general characteristics may be deduced. If the nature of the nonlinearity is such that N increases monotonically as A increases [curve (1), Fig. 14], then an unstable limit cycle is indicated. However, if N increases but approaches a limit asymptotically as A increases, the limit cycle will occur only if the asymptote has a value of $k_1 N_{LC}$ corresponding to the limit cycle [for curve (2), the value is less, so no limit cycle is indicated]. If N decreases monotonically as A increases,

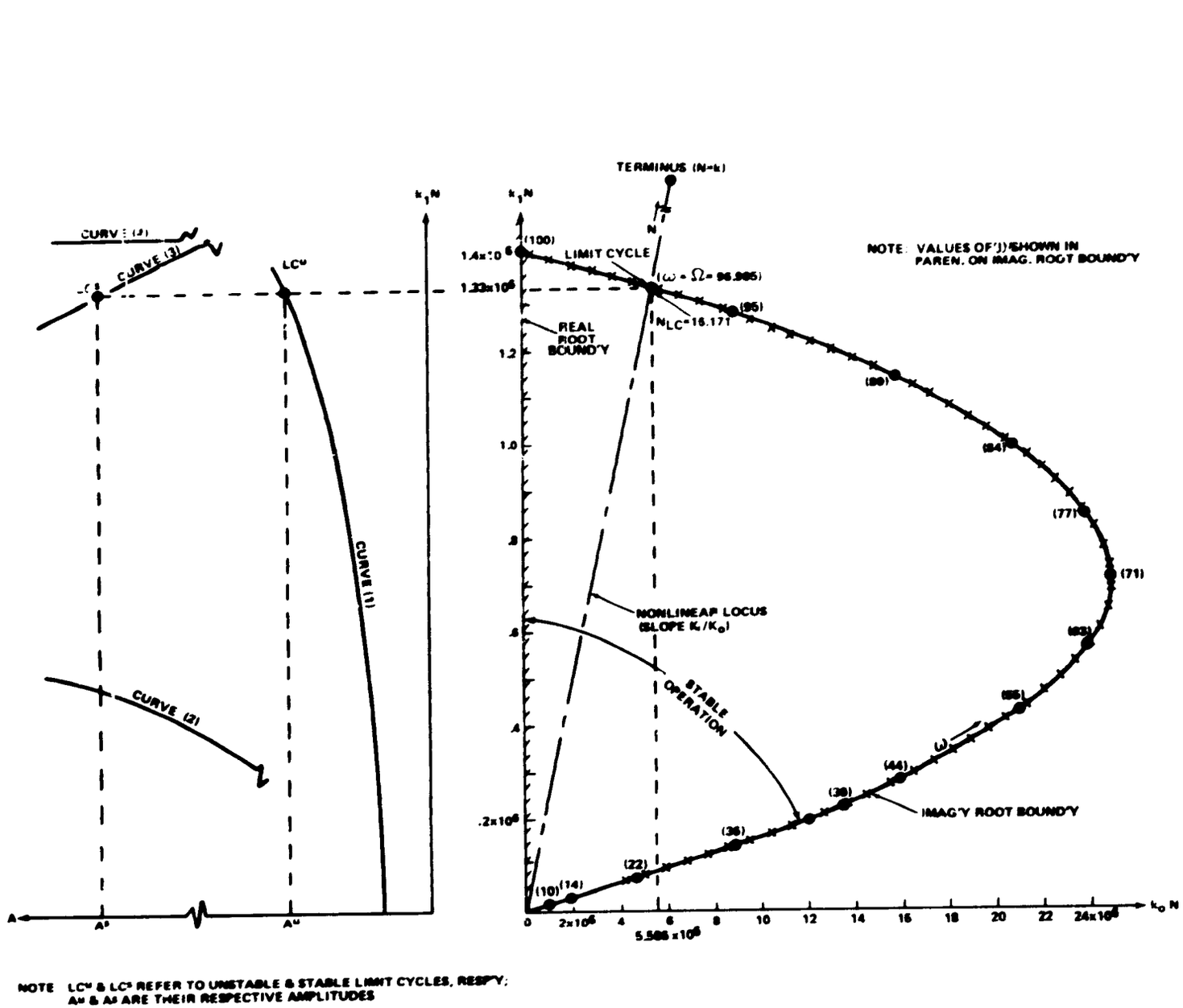

NOTE LC^u & LC^s REFER TO UNSTABLE & STABLE LIMIT CYCLES, RESP'Y;
A^u & A^s ARE THEIR RESPECTIVE AMPLITUDES

Figure 14. Case II (Bendix model number 1) — stability characteristics.

a stable limit cycle will occur as long as the curve of k_1N versus A begins at a value greater than k_1N_{LC} [e.g., curve (3)]. If the curve remains above the value of k_1N_{LC} for all A [curve (4)], no limit cycle will occur. These observations lead to an investigation of describing function characteristics for various appropriate nonlinearities.

Limit Case 1 (Ideal Relay). Since N decreases monotonically as A increases, a stable limit cycle is indicated with an amplitude [see equation (12)]

$$A = 4M/N\pi \quad . \tag{29}$$

[N is obtained from equation (27) and frequency Ω is obtained from equation (28).]

If the numerical values of Table 1 are used,

$$N = 16.1707 \quad , \tag{30}$$

$$\Omega = 96.985 \text{ rad/s} = 15.4357 \text{ Hz} \quad . \tag{31}$$

If, for example, M is chosen as 0.055, a value of $A^s = 0.00434$ is predicted.[3] The amplitude NA of the assumed sine wave f(x) is NA = 0.07018. The amplitude of $|\theta|_{LC}$ and $|\dot{\theta}|_{LC}$ of oscillations in θ and $\dot{\theta}$ may be determined from this relationship with the signal x (Fig. 1). Assuming the form of equation (3) for x, the amplitude of the θ limit cycle $|\theta|_{LC}$ and the $\dot{\theta}$ limit cycle $|\dot{\theta}|_{LC}$ may be approximated by

$$|\dot{\theta}|_{LC} = \frac{A}{K_1} \tag{32a}$$

3. Superscripts u and s refer to quantities associated with unstable and stable limit cycles, respectively.

and

$$|\theta|_{LC} = \frac{|\dot{\theta}|_{LC}}{\Omega} \quad . \tag{32b}$$

Using equations (32), amplitudes of $|\theta|_{LC}$ and $|\dot{\theta}|_{LC}$ are found to be 4.0123×10^{-11} rad and 3.891×10^{-9} rad/s, respectively.

Limit Case 2(Relay With Dead Zone). In this case stable operation without a limit cycle is indicated if $DN/M < 2/\pi$. If $DN/M > 2/\pi$, both a stable limit cycle and an unstable limit cycle are predicted, since the curve of k_1N versus A rises above the value of k_1N_{LC} to a peak value and then falls below it. A case of academic interest arises when DN/M is precisely equal to $2/\pi$. In that case, a semistable limit cycle will occur. Using a value of $M = 0.55$ and $D = 0.0011$, equation (13) may be solved for the two predicted values of A, $A^u_s = 0.00114$ and $A^s = 0.0042$, and amplitudes of f(x), $NA^u = 0.0184$ and $NA^s = 0.0679$. From equation (32), θ and $\dot{\theta}$ limit cycle magnitudes are found to be $|\theta|^u_{LC} = 1.0539 \times 10^{-11}$ rad, $|\dot{\theta}|^u_{LC} = 1.0221 \times 10^{-9}$ rad/s.

Limit Case 3 (Gain With Dead Zone). It is seen from equation (14) and Figures 13 and 14 that an unstable limit cycle will occur if $k > N$, and stable operation will occur if $k < N$. An example is obtained by setting $k = 20$. If $D = 0.011$, equation (14) may be solved for the predicted value of A: $A^u = 0.0729$. From equation (32), $|\theta|^u_{LC} = 6.7396 \times 10^{-10}$ rad and $|\dot{\theta}|^u_{LC} = 6.5364 \times 10^{8}$ rad/s. Amplitude of f(x) then becomes $NA^u = 1.1788$. If $D = 0.00022$, then $A^u = 0.00146$, $NA = 0.02361$, $|\theta|^u_{LC} = 1.3498 \times 10^{-11}$ rad, and $|\dot{\theta}|^u_{LC} = 1.3091 \times 10^{-9}$ rad/s.

Limit Case 4 (Preload). It is apparent from equation (15) and Figures 9 and 14 that a stable limit cycle is predicted if $k < N$ and that unstable operation will occur if $k > N$. An example of the effect of a preload characteristic nonlinearity is obtained by setting $k = 1$, $M = 0.055$. Solving equation (15) for A, one predicts $A^s = 0.004616$ and $NA^s = 0.07464$. From equation (32), $|\theta|^s_{LC} = 4.267 \times 10^{-11}$ rad and $|\dot{\theta}|^s_{LC} = 4.1388 \times 10^{-9}$ rad/s.

the value of asymptote $N/k = 1$ when $\xi > 1$ $(k > M/D)$. Using the same means of analysis as used in the preceding cases, numerical examples corresponding to each of these six conditions are developed. They are summarized with the results of the numerical examples of the five limit cases in Table 2. Attention is directed to the case covered by Condition 1 where $M = D$, $k = 1$: This is the set of conditions on the nonlinearity that is used in References 4 through 6 and footnote 2 and is reported as causing limit cycles. The analysis contained herein disagrees with the reported results in that this analysis predicts stable operation and the absence of any limit cycles.

Analysis of Case III

The characteristic equation is

$$s^4 + (\omega_c + \omega_g)\, s^3 + \omega_c \omega_g s^3 + \omega_c (\bar{K}_1 \omega_g + \bar{K}_0) \frac{Ns}{I_v}$$

$$+ \omega_c \omega_g \bar{K}_0 \frac{N}{I_v} = 0 \quad , \tag{34}$$

where overbars are used on gains K_0 and K_1 to identify them with the system of equation (34) rather than Case II. Comparing equation (34) to equation (21), one can immediately draw conclusions from the analysis associated with the system represented by equation (21). Matching the terms,

$$g_1 = \omega_c + \omega_g \quad , \tag{35a}$$

$$g_0 = \omega_c \omega_g \quad , \tag{35b}$$

$$k_0 = \bar{K}_0 g_0 / I_v \quad , \tag{35c}$$

and

$$k_1 = \omega_c (\bar{K}_0 + \omega_g \bar{K}_1) / I_v \quad . \tag{35d}$$

Limit Case 5 (Gain Change). For the anticipated values of $m \ll k$, equation (16) is approximated by equation (14). It is anticipated that the results of the analysis of Limit Case 3 will apply approximately to Limit Case 5.

Basic Nonlinearity (Fig. 1). The effect of varying the basic nonlinearity's parameters k, M, and D will be investigated in detail. An examination of Figures 7 and 14 yields most of the following information:

Condition 1. $N > k \geq M/D$: Stable operation (no limit cycle).

Condition 2. $N > k < M/D > k/\xi_0$: Two limit cycles; one stable, one unstable with $A^u < A^s$.

Condition 3. $N > k < M/D < k/\xi_0$: Stable operation (no limit cycle).

Condition 4. $N = k > M/D$: Unstable limit cycle.

Condition 5. $N = k < M/D$: Unstable limit cycle.

Condition 6. $N > k < M/D = k/\xi_0$: Semistable limit cycle.

Additional information was needed to obtain the inequality relationships between M/D and k/ξ_0 for conditions 2, 3, and 6. From equation (11), it is seen that a peak in N/k versus A/D can occur only when

$$\xi > 2 \tag{33a}$$

or

$$\xi = 1 \quad . \tag{33b}$$

Since D/A must be less than unity for equation (10a) to be applicable, it is seen from equation (11) that inequality (33a) is meaningless physically. Also from equation (10b), it is seen that $\xi > 0$. To summarize, N/K will have a peak only when $0 < \xi < 1$ $(k < M/D)$ and will approach but not exceed

TABLE 2. SUMMARY OF BENDIX MODEL NUMBER 1 RESULTS

Case	Nonlinearity	k	D	M	Analytical Predictions[a,b] A	Analytical Predictions[a,b] NA	Analytical Predictions[a,b] $\dot{\theta}_{i_{LC}}$ (rad)	Analytical Predictions[a,b] $\dot{\theta}_{i_{LC}}$ (rad/s)	Simulation Results A	Simulation Results NA	Simulation Results $\dot{\theta}_{i_{LC}}$	Simulation Results $\dot{\theta}_{i_{LC}}$
II	Ideal Relay (Figs. 18 and 19)	0	0	0.055	0.00434[s]	0.07018[s]	4.0123×10^{-11}	3.891×10^{-9}	0.014[s]	0.055[s]	5×10^{-11}	4×10^{-9}
	Relay with Dead Zone (Fig. 20)	0	0.0011	0.055	0.00114[u] 0.0042[s]	0.01843[u] 0.0679[s]	1.0539×10^{-11} 3.8829×10^{-11}	1.0221×10^{-9} 3.766×10^{-9}	Not Detectable 0.00425	0.055	1×10^{-10}	4×10^{-9}
	Gain Change with Dead Zone	20	0.011	0	0.0729[u]	1.1788[u]	6.7396×10^{-10}	6.5364×10^{-8}	c			
			2.2×10^{-4}	0	0.00146[u]	0.02361[u]	1.3498×10^{-11}	1.3091×10^{-9}	c			
	Preload (Figs. 21 and 22)	1	0	0.055	0.004616	0.07464	4.2675×10^{-11}	4.1388×10^{-9}			5×10^{-11}	3.5×10^{-9}
	Basic Nonlinearity 1a $N > k = M/D$ (Fig. 23)	1	0.011	0.011	Stable Response				Stable Response		N/A	N/A
			2.2×10^{-4}	2.2×10^{-4}	Stable Response				c			
	1b $N > k > M/D$	1	0.0545	0.011	Stable Response				Stable Response		N/A	N/A
			1.089×10^{-3}	2.2×10^{-4}	Stable Response				c			
	2 $N > k < M/D > k/\delta_0$ (Figs. 24 and 25)	4.95	0.011	0.275	0.0142[u] 0.0204[s]	0.2296[u] 0.3299[s]	1.3128×10^{-10} 1.8860×10^{-10}	1.2732×10^{-8} 1.8291×10^{-8}	0.013[u] 0.023[s]	0.28[u] 0.34[s]	— 2×10^{-10}	1×10^{-8} 2×10^{-8}
			2.2×10^{-4}	0.00550	0.000285[u] 0.00041[s]	0.004609[u] 0.006630[s]	2.6348×10^{-12} 3.7904×10^{-12}	2.5554×10^{-10} 3.6761×10^{-10}	c			
	3 $N > k < M/D < k/\delta_0$ (Fig. 26)	0.95	0.011	0.011	Stable Response				Stable Response		N/A	N/A
			2.2×10^{-4}	2.2×10^{-4}	Stable Response				c			
	4 $N < k > M/D$ (Fig. 27)	20	0.011	0.011	0.068[u]	1.0996[u]	6.2866×10^{-10}	6.0970×10^{-8}	0.06[u]	0.63[u]	6×10^{-10}	5.5×10^{-8}
			2.2×10^{-4}	2.2×10^{-4}	0.00138[u]	0.02232[u]	1.2758×10^{-11}	1.2373×10^{-9}	c			
	5. $N < k < M/D$ (Fig. 28)	20	0.011	0.275	0.0131[u]	0.2118[u]	1.2111×10^{-10}	1.1746×10^{-8}	0.012[u]	0.58[u]	Not Detectable	
			2.2×10^{-4}	0.00550	0.000263[u]	0.004253[u]	2.4314×10^{-12}	2.3581×10^{-10}	c			
	6 $N < k < M/D = k/\delta_0$ (Fig. 29)	1	0.011	0.2763	0.015717[u,s]	0.025415[u,s]	1.4530×10^{-10}	1.4092×10^{-8}	0.016[u,s]	0.26[u,s]	$\sim 2 \times 10^{-10}$	1.5×10^{-8}
			2.2×10^{-4}	0.00550	0.0003143[u,s]	0.0050830[u,s]	2.9061×10^{-12}	2.8184×10^{-10}	c			
IV	Basic 1a $N > k = M/D$	1	0.011	0.011	Stable Response				c			
	1b $N > k > M/D$	1.5	0.011	0.011	Stable Response				c			
	2 $N > k < M/D > k/\delta_0$	2	0.011	0.044	0.0123[u] 0.270[s]	0.0258[u] 0.567[s]	1.1371×10^{-10} 2.4961×10^{-9}	1.1028×10^{-8} 2.4209×10^{-7}	c			
	4 $N < k > M/D$	5	0.011	0.011	0.0188[u]	0.0395[u]	1.7380×10^{-10}	1.6856×10^{-8}	c			
	5 $N < k < M/D$	5	0.011	0.0825	0.01128[u]	0.0237[u]	1.0428×10^{-10}	1.01139×10^{-8}	c			
	6 $N > k < M/D = k/\delta_0$	1	0.011	1/0.16	0.016[u,s]	0.0336[u,s]	1.4792×10^{-10}	1.4345×10^{-8}	c			

a. In all runs, predicted and measured values of Ω were identical. Case II $\Omega = 15.4357$ Hz; Case IV $\Omega = 6.519$ Hz

b. Superscripts u, s, us indicate values are associated with unstable, stable, or semistable limit cycles, respectively

c. Indicates runs not confirmed by simulation

Now, equations (21) through (26) may be used directly for this model. Hence, it is seen that the effect of ω_g — i.e., a nonideal rate gyro — is to introduce the possibility of a limit cycle, considering Conditions 1-6 listed previously. A numerical example is selected using the values in Table 1, yielding $N = 9.69$ and $\Omega = 40.64$ rad/s. If a nonlinearity of $M = D$ and $k = 1$ is chosen, it is again seen (Condition 1) that limit cycle operation will not occur. The analysis used in Case II and summarized in Table 2 is directly applicable to this case as well.

Analysis of Case IV

The characteristic equation is

$$s^5 + (g_1 + \omega_g)s^4 + (g_0 + \omega_g g_1)s^3 + \omega_g g_0 s^2 + (\omega_g \beta + \alpha)Ns + \omega_g \alpha N = 0 \quad , \tag{36}$$

where

$$\alpha \stackrel{d.}{=} K_0 K_G / I_v \tag{37a}$$

and

$$\beta \stackrel{d.}{=} K_1 K_G / I_v \quad . \tag{37b}$$

The stable region, in terms of an $\alpha N - \beta N$ parameter plane, is bounded by the real root boundary

$$\alpha N = 0 \tag{38}$$

and the imaginary root boundary

$$\alpha N = \omega^2 \left[g_0 - \left(1 + \frac{g_1}{\omega_g} \right) \omega^2 \right] \quad , \tag{39a}$$

and

$$\beta N = g_1 \omega^2 \left(1 + \omega^2 / \omega_g{}^2 \right) \tag{39b}$$

Again, the nonlinear locus is the straight line determined by equation (39):

$$\beta N = (K_1/K_0)\, \alpha N \quad . \tag{40}$$

This is shown in Figure 15. If a limit cycle is to occur, it will have the characteristics associated with the intersection of the boundary defined by equations (39) and the nonlinear locus [equation (40)]. Using the numerical values of Table 1 to solve equations (39) and (40) simultaneously leads to

$$N = 2.103 \tag{41}$$

and

$$\Omega = 40.959 \text{ rad/s} = 6.519 \text{ Hz} \quad . \tag{42}$$

The six conditions listed previously may be used to analyze the possibility of limit cycle operation. Again, it may be readily concluded that for $M = D$ and $k = 1$, limit cycle operation will not occur. Limit cycle characteristics for other values of M, D, and k may be predicted, however. Examples are summarized in Table 2.

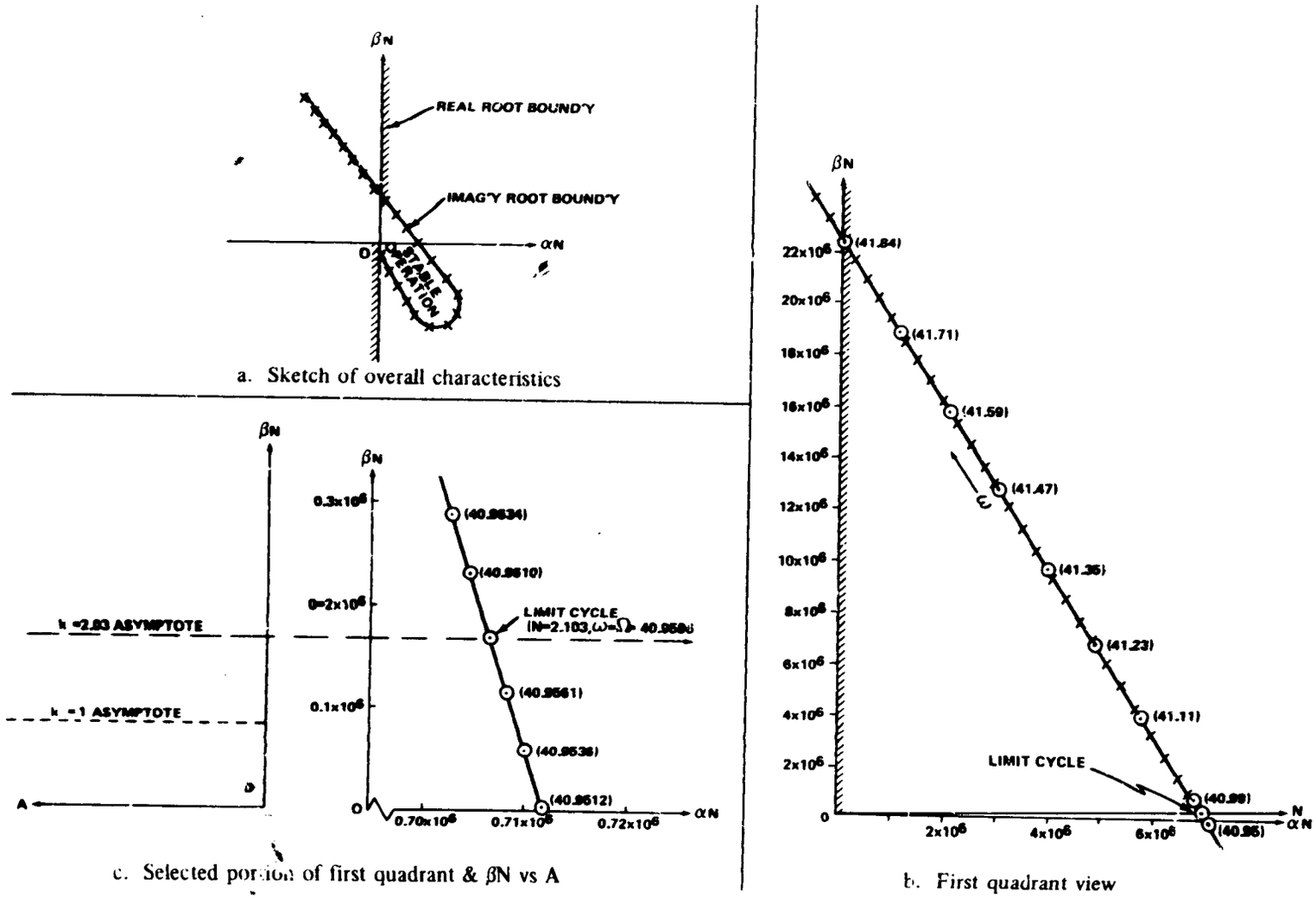

Figure 15. Case IV (Bendix model number 1) — stability characteristics.

Most of the results presented above for Bendix model number 1 have been confirmed by analogue simulation.[4] The model of Figure 1 was set up on the EAI 231R-V computer in the Astrionics Laboratory at Marshall Space Flight Center. The simulation diagram used is shown in Figure 16, and the nonlinearity used on the computer is shown in Figure 17. This simulation description is detailed and lengthy because it graphically portrays numerous combinations of unusual limit cycles normally found only in textbooks.

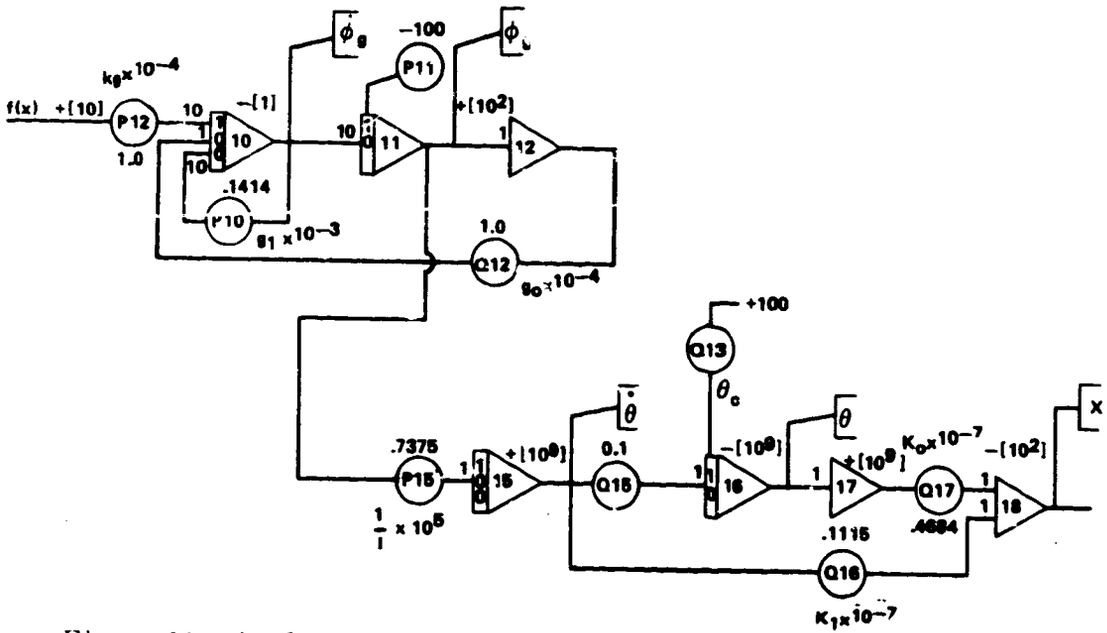

Figure 16. Analogue simulation diagram for Bendix model number 1.

Simulation of Case I

Several simulation runs were made to confirm the predicted stable behavior of the system. The simplicity of the results does not warrant reproduction herein, so they are omitted.

Simulation of Case II

This case provides the basis of the results reported herein and is described in detail. The tabulated results (Table 2) will assist the reader in following the discussion.

4. The results presented in this section are due to the efforts of Mr. P. H. Fisher, Guidance and Control Systems Branch, Systems Division, Astrionics Laboratory, MSFC, who worked with the author to confirm the analytically derived results. His contributions are gratefully acknowledged.

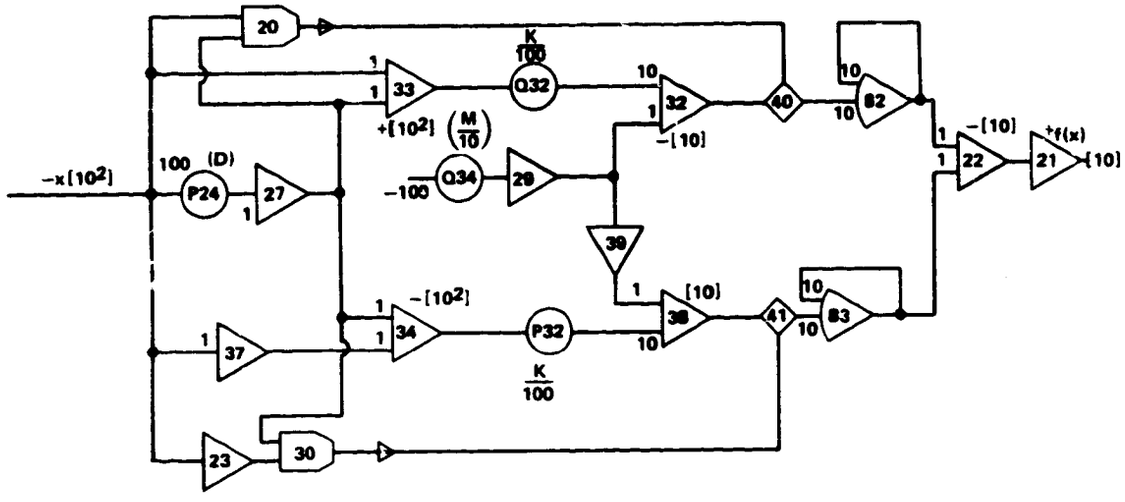

Figure 17. Analogue simulation diagram for CMG nonlinearity of Bendix model number 1.

Limit Case 1 (Ideal Relay). A stable limit cycle is predicted and is confirmed in Figures 18 and 19. In Figure 18, the limit cycle trajectory is approached from within (in a state space sense) with $x(0) < A^S$, and in Figure 19 the limit cycle trajectory is approached from the outside with $x(0) > A^S$. Hence, the stability of the limit cycle is demonstrated. The steady state amplitudes of x, i.e., A^S, θ and $\dot{\theta}$, may be read directly from Figures 18 and 19 and are tabulated in Table 2 for comparison with the predicted values. Only the value of the magnitude of f(x) varies appreciably from predicted values because of its assumed (for describing function analysis purposes) sinusoidal shape. The frequency of the sustained oscillation closely matches the predicted frequency (Ω) in this case and all other Case II simulations.

Limit Case 2 (Relay With Dead Zone). Both the unstable and stable limit cycles are predicted for this case. The amplitude of A was too small (i.e., too nearly identical to dead zone D) to be observed. However, the stable limit cycle was detected and its nature confirmed. A sample run, with $x(0) > A^S$, is shown in Figure 20.

Limit Case 3 (Gain With Dead Zone). Because of the close agreement between analytical and simulation results in other cases, this case was not simulated.

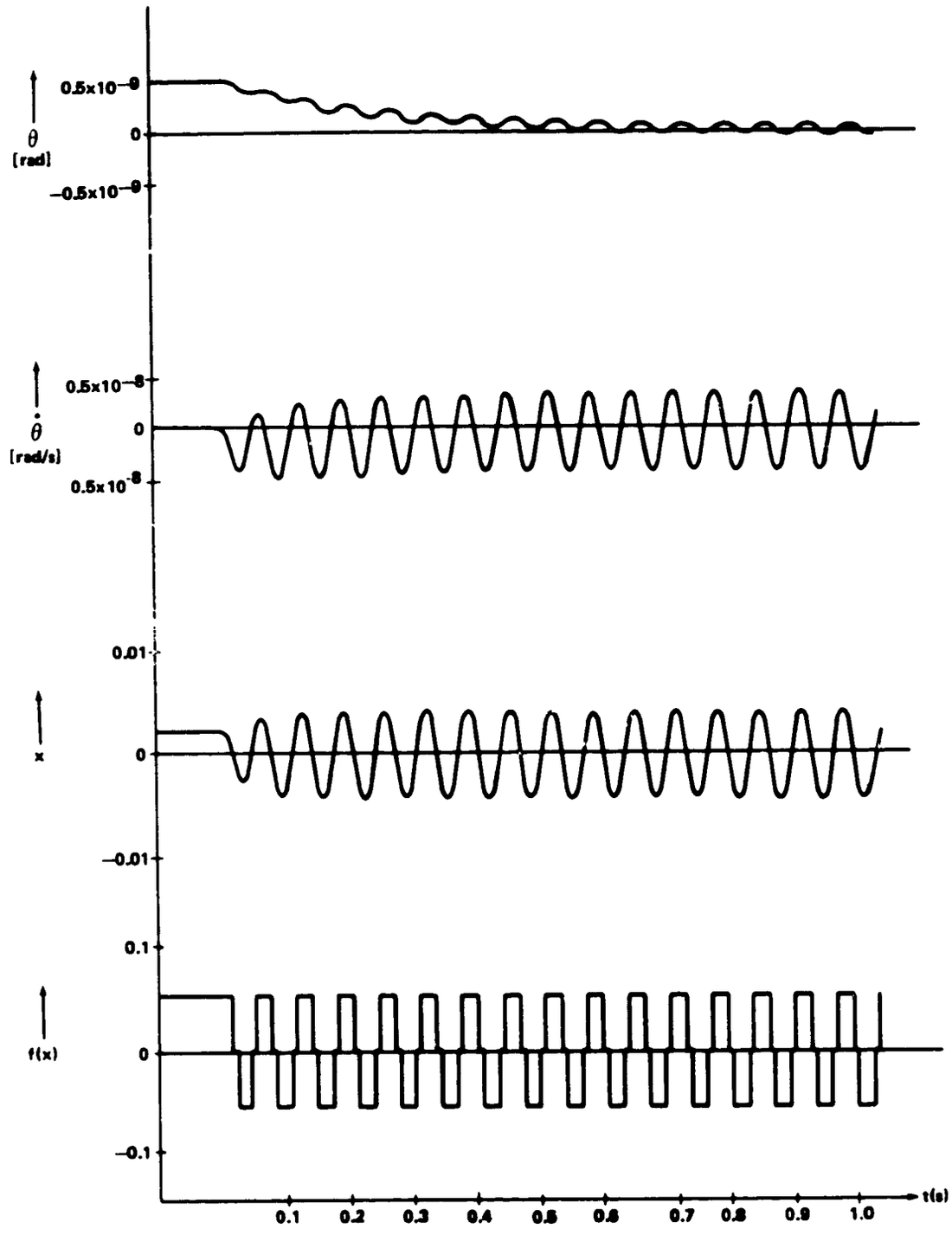

Figure 18. Limit Case 1 (Ideal Relay) simulation, M = 0.055: $x(0) < A^S$.

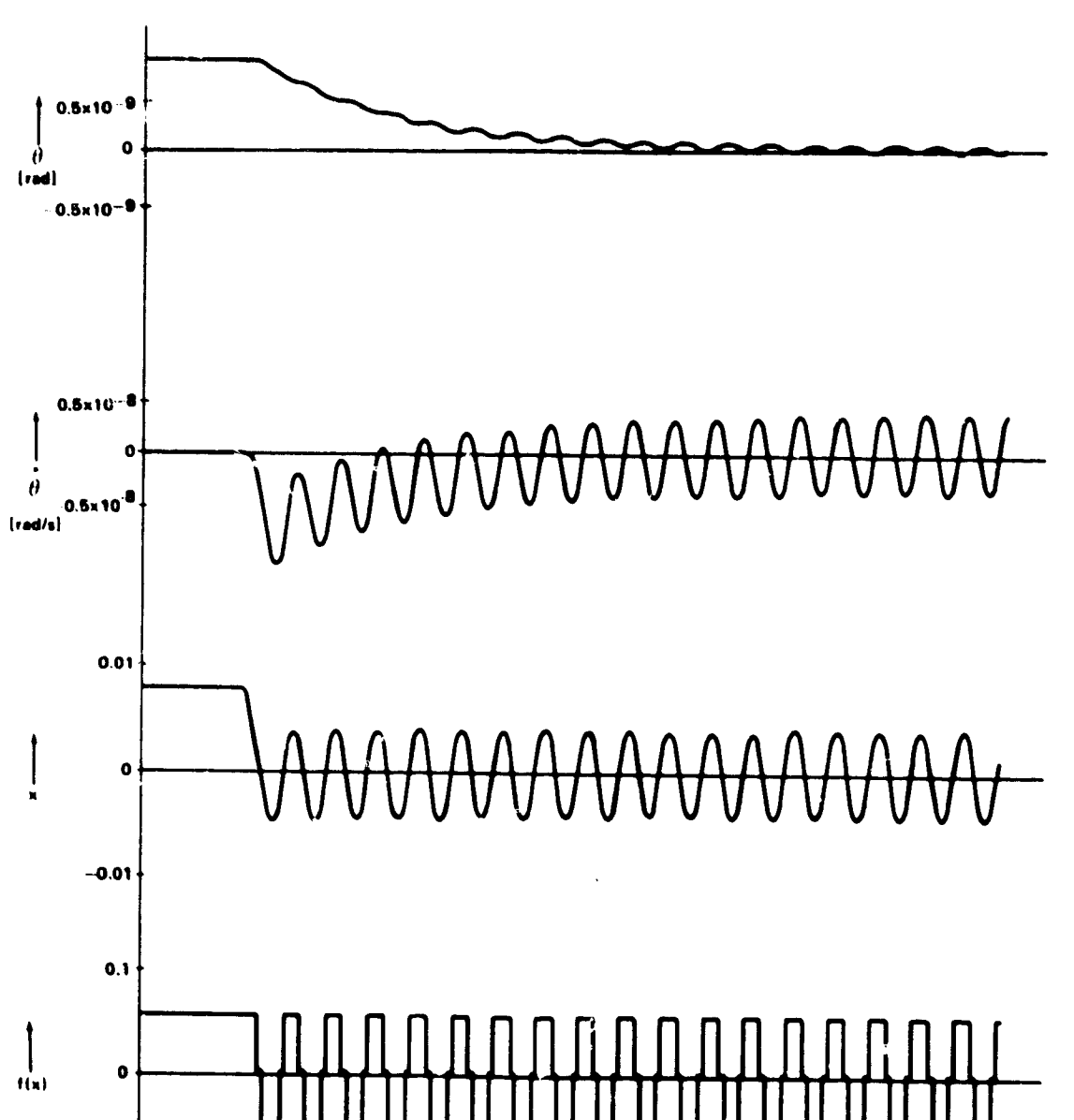

Figure 19. Limit Case 1 (Ideal Relay) simulation, M 0.055: $x(0) > A^s$.

Limit Case 4 (Preload). This is another case of a predicted stable limit cycle. Similar to the approach of Limit Case 1, the predicted stable limit cycle characteristics are confirmed in Figures 21 and 22.

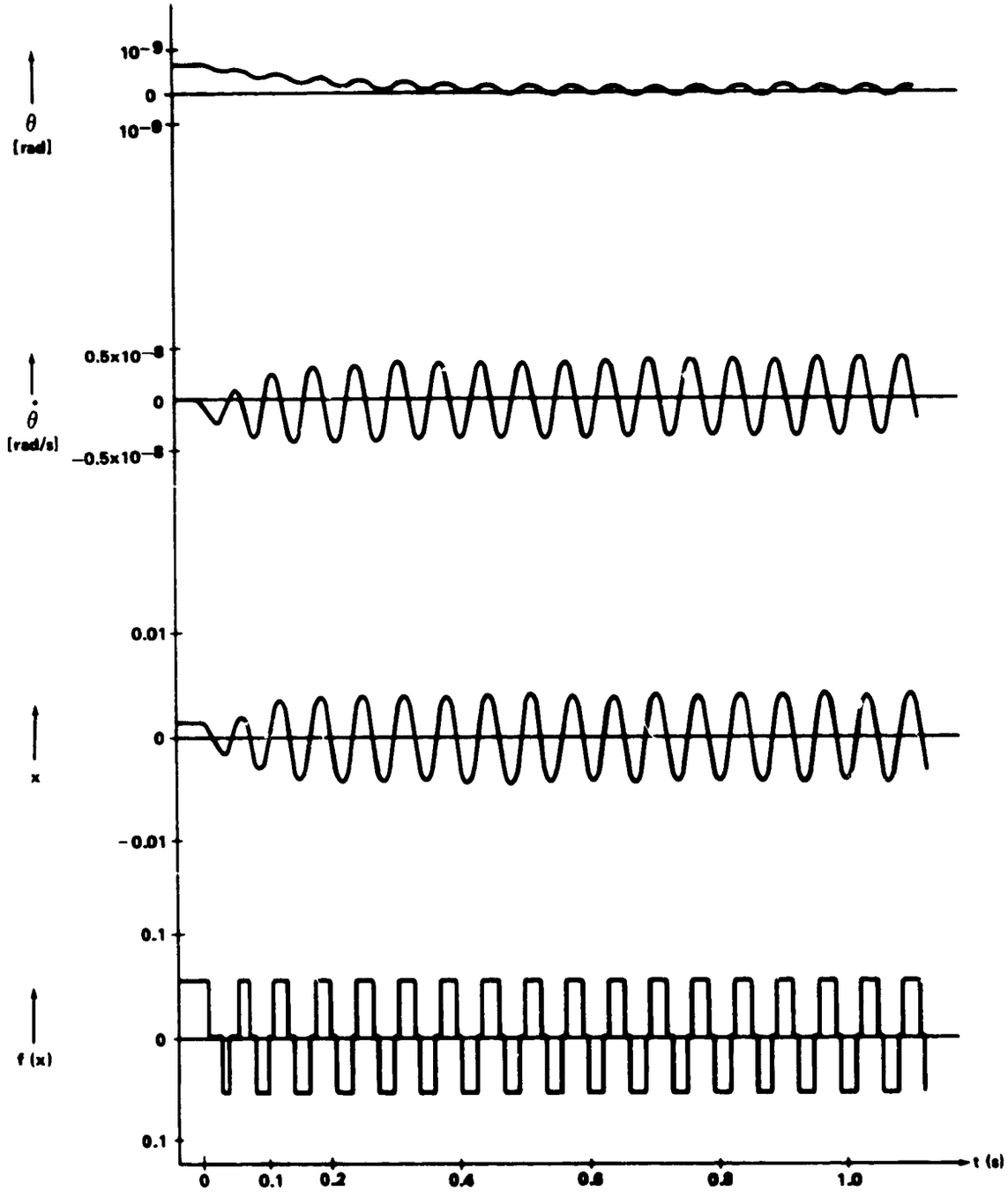

Figure 20. Limit Case 2 (Ideal Relay with Dead Zone) simulation, $D = 0.0011$, $M = 0.055$: $x(0) < A^S$.

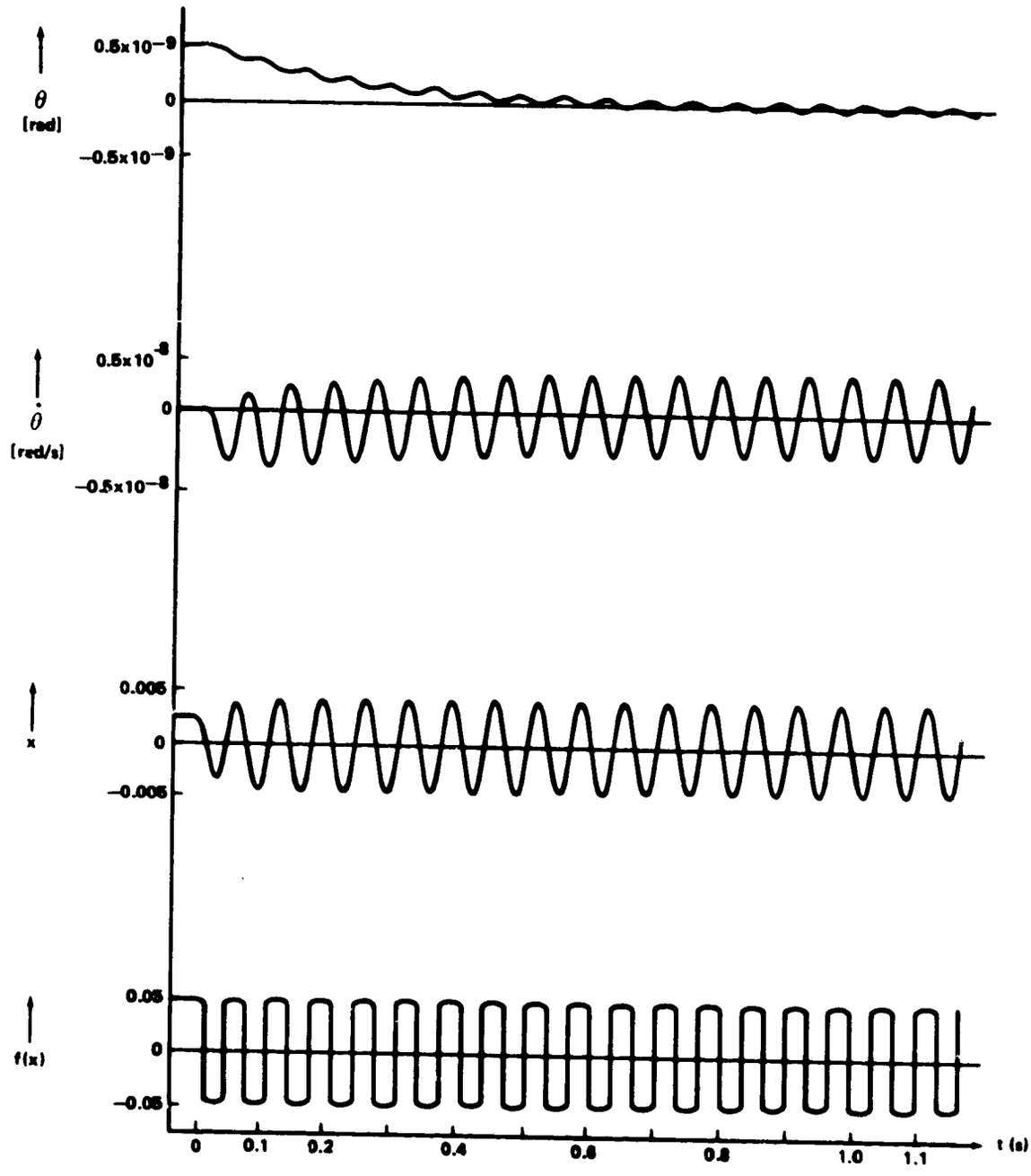

Figure 21. Limit Case 4 (Preload) simulation, k = 1, M = 0.055: $x(0) < A^s$.

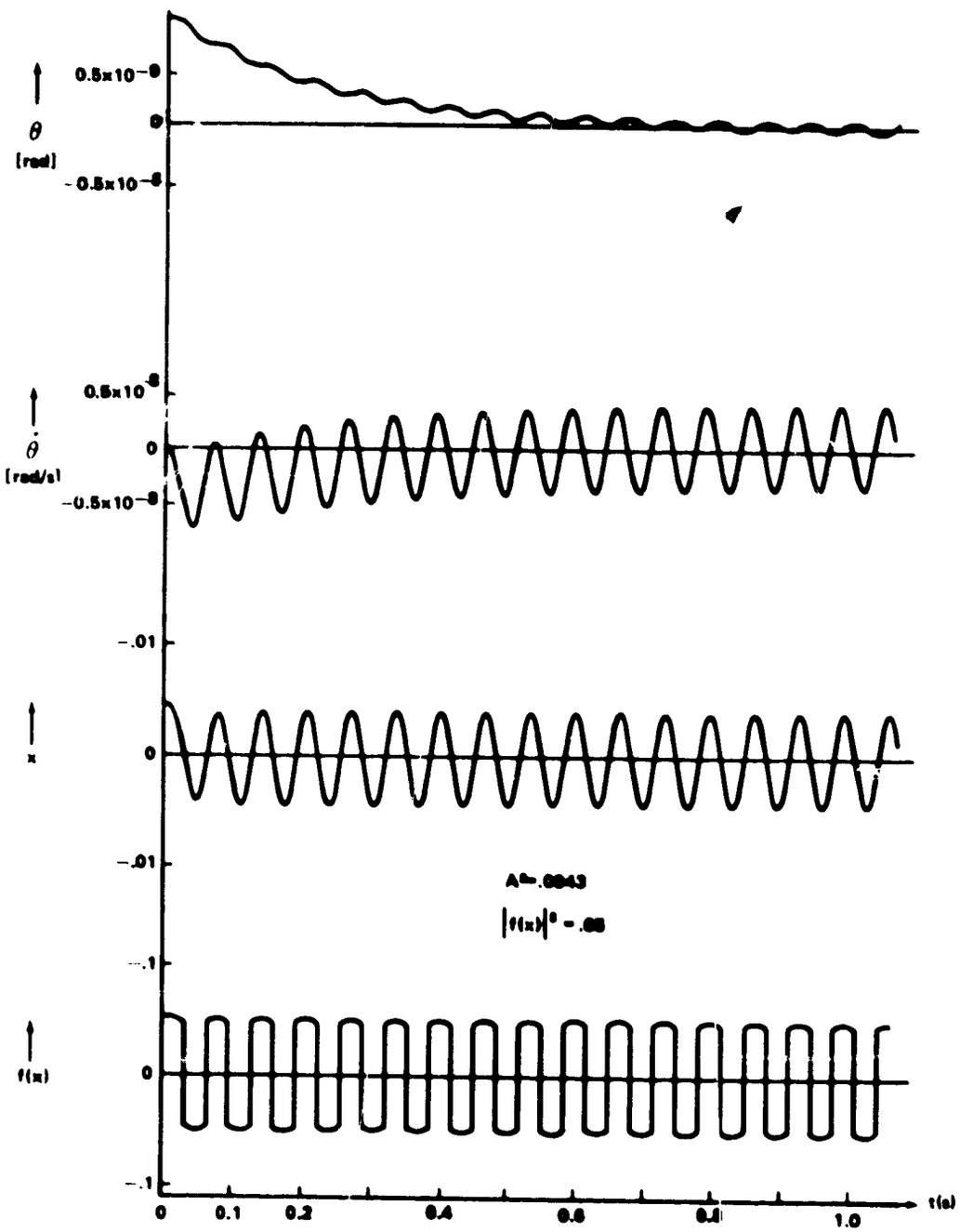

Figure 22. Limit Case 4 (Preload) simulation, k = 1, M = 0.055: $x(0) > A^s$.

Limit Case 5 (Gain Change). This case, similar to Limit Case 3 since $m \ll k$, was not simulated.

Basic Nonlinearity

Condition 1 ($N > k \geq M/D$). As predicted and indicated in Figure 23, all initial conditions within the limits of scaling resulted in stable operation.

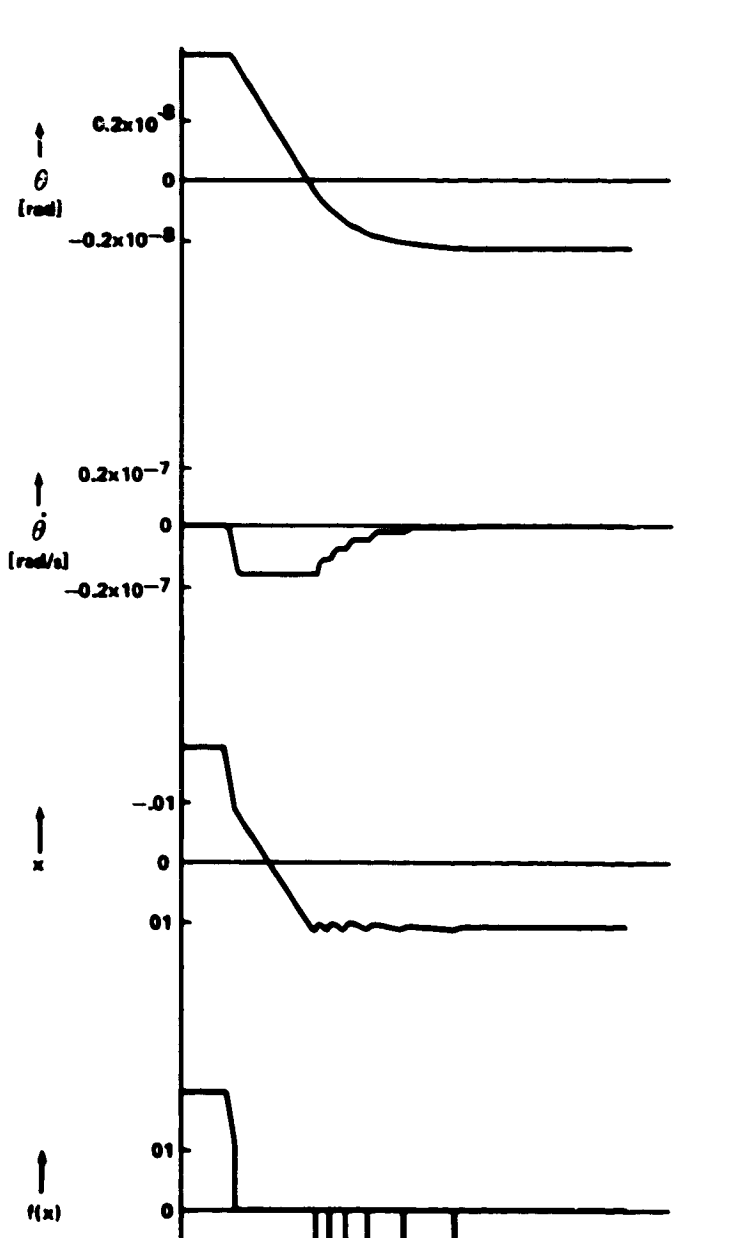

Figure 23. Basic nonlinearity simulation, k = 1, D = M = 0.011.

Condition 2 ($N > k < M/D > k/\xi_0$). In this condition (as in Limit Case 2) both unstable and stable limit cycles are predicted. As in the nature of unstable limit cycles, it is extremely difficult to maintain their oscillations. However, Figure 24 contains a good example of an unstable limit cycle maintained for several periods before the trajectory escapes to the sustained oscillation of the stable limit cycle ($A^S > A^u$). In another run (not included in report), the unstable nature of the limit cycle was seen as the states decreased to zero. The stable nature of the larger amplitude cycle is confirmed in Figure 25 where $x(0) > A^S$.

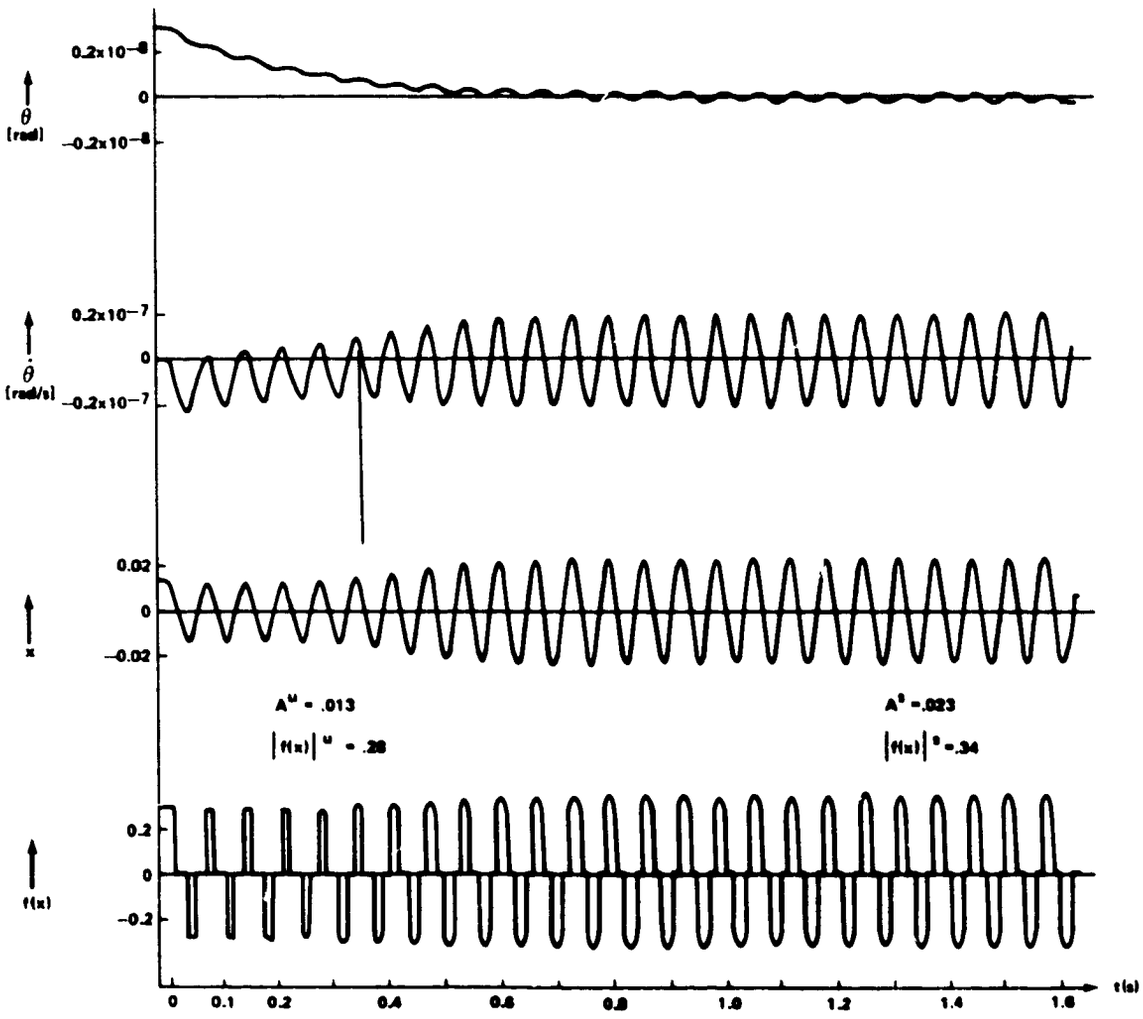

Figure 24. Basic nonlinearity simulation, k = 4.95, D = 0.011, M = 0.275: $x(0) < A^u$.

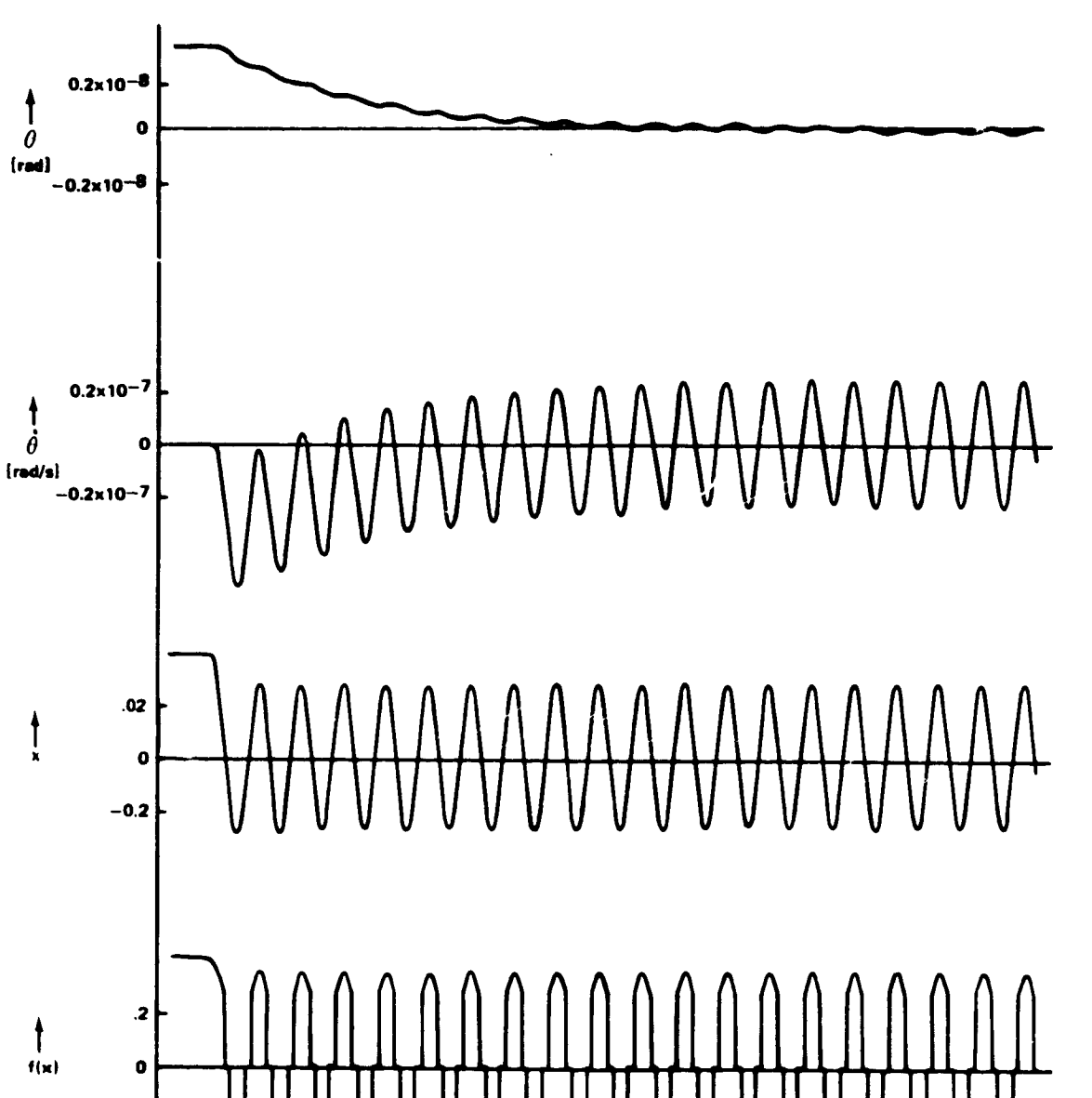

Figure 25. Basic nonlinearity simulation, $k = 4.95$, $D = 0.011$, $M = 0.275$: $x(0) > A^{s}$.

Condition 3 ($N > k > M/D > k/\xi_0$). As predicted, stable operation ensues (Fig. 26).

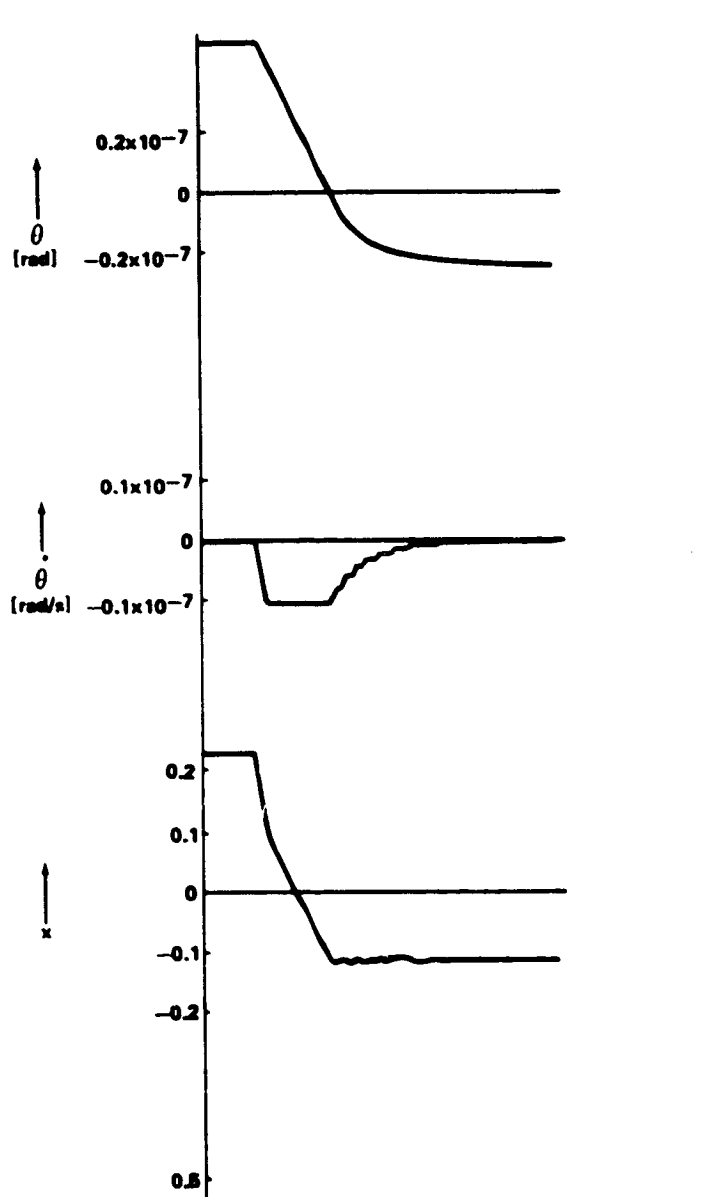

Figure 26. Basic nonlinearity simulation, k = 0.95, D = M = 0.011.

Condition 4 ($N < k > M/D$). This case (Fig. 27) provides an unusually good example of an unstable limit cycle maintaining a sustained oscillation for a large number of periods before (in this case) the response diverges from the limit cycle trajectory.

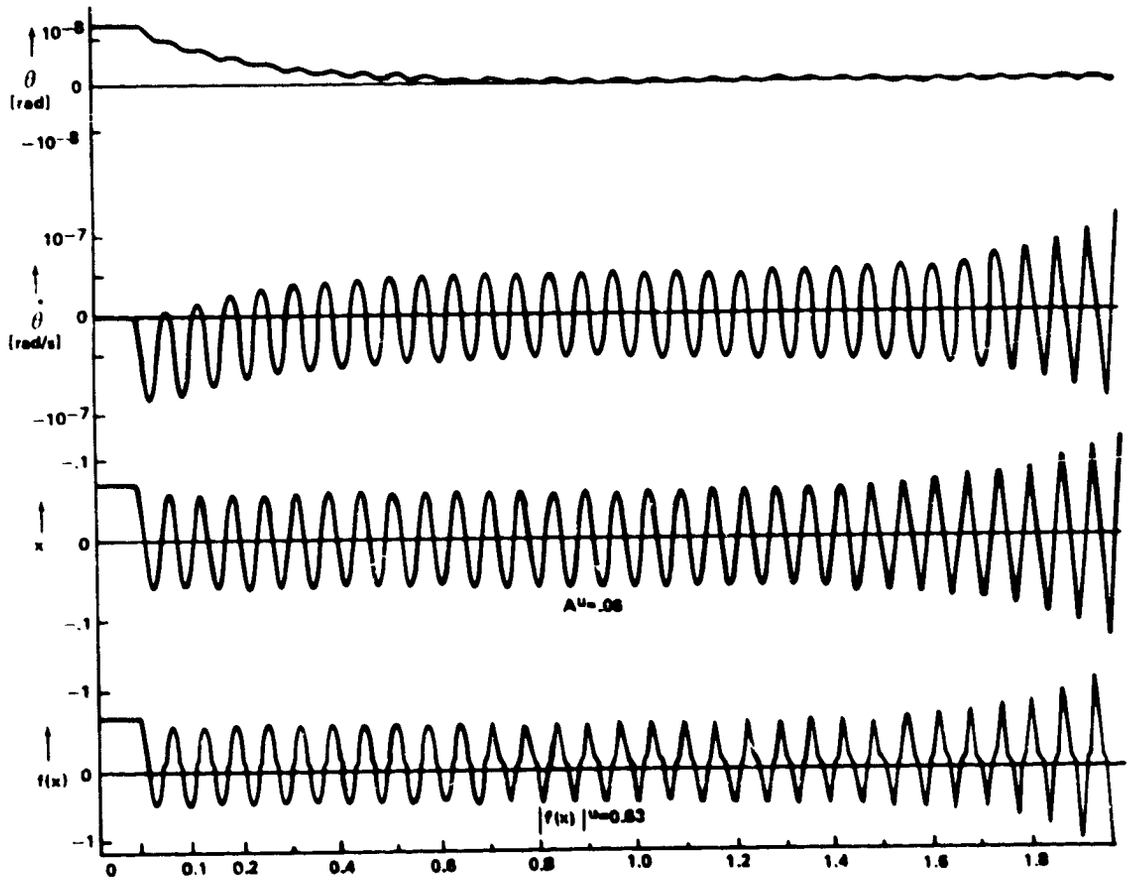

Figure 27. Basic nonlinearity simulation, k = 20, D = M = 0.011

Condition 5 ($N < k < M/D$). Figure 28 is an example of an unstable limit cycle. The first run shows the elusive unstable limit cycle trajectory rapidly diverging to a stable response. The second run shows the trajectory, just as quickly, diverging to an unstable response.

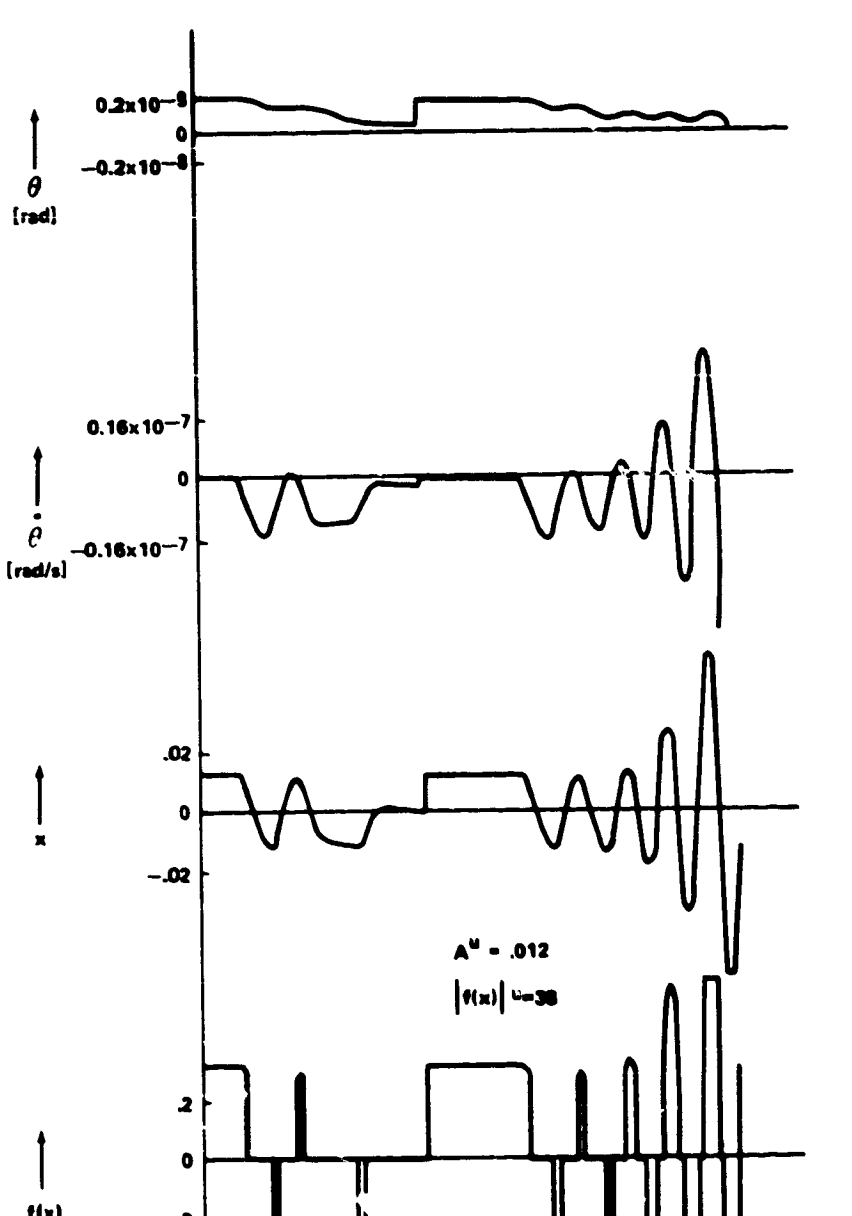

Figure 28. Basic nonlinearity simulation, k = 20, D = 0.011, M = 0.275

Condition 6 $(N < k < M/D = K/\xi_0)$. This run (Fig. 29) confirms the predicted behavior of a stable limit cycle and an unstable limit cycle merged into one, yielding a semistable limit cycle. In this run, $x(0) > A^{u,s}$ and the system response approaches and maintains the limit cycle behavior. After a number of cycles elapse, however, the response leaves the limit cycle trajectory to assume a stable response. Hence, the limit cycle is stable when the trajectory is approached from outside and unstable when approached from inside.

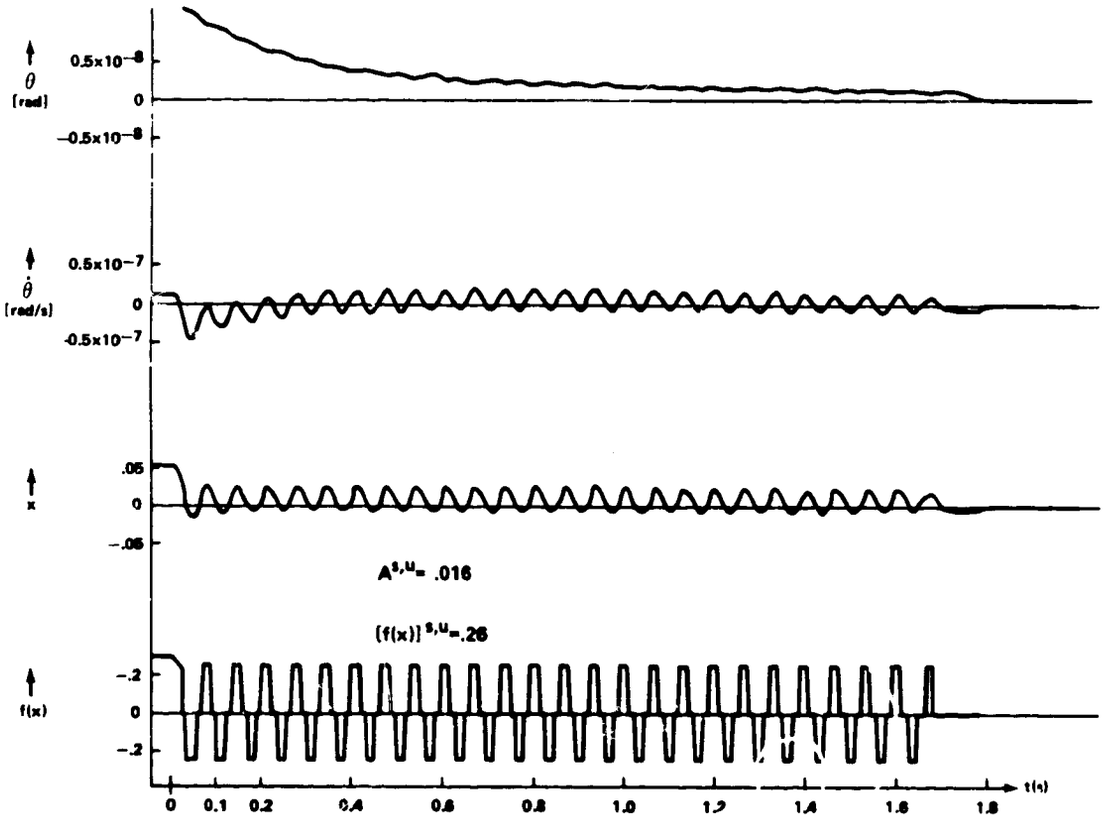

Figure 29. Basic nonlinearity simulation, k = 1, D = 0.011, M = 0.257: $x(0) > A^{u,s}$.

Simulation of Case III

Because of the close relationship to Case II, this case was not simulated.

Simulation of Case IV

This case should have been confirmed by simulation but was concluded because of time constraints.

Summary

Because the describing function technique assumes that the input and output to the nonlinearity are both sinusoidal in nature, it is to be expected that the actual magnitudes of these transcendental functions will only be approximated by the mathematical estimates. The closeness of the predictions to the simulation results is surprisingly accurate, considering the shape of the waveforms at the output of the nonlinearity. The predicted time periods were particularly accurate.

ANALYSIS OF SPERRY MODEL (Fig. 2)

A brief (compared to the preceding analysis) analysis was made of the Sperry model that was presented to MSFC in December 1972. The characteristic equation associated with the model is

$$\frac{I_v I_{GE}}{k_F} s^5 + I_v\left(\frac{\kappa_1}{k_F} + I_{GE}N\right) s^4 + \left[I_v\left(\frac{\kappa_0}{k_F} + 1 + \kappa_1 N\right) + HK_1\frac{\kappa_1}{k_F}\right] s^3$$

$$+ \left[I_v\kappa_0 N + HK_1\left(\frac{\kappa_0}{k_F} + \kappa_1 N\right) + HK_0\frac{\kappa_1}{k_F}\right] s^2$$

$$+ H\left[K_1\kappa_0 N + K_0\left(\frac{\kappa_0}{k_F} + \kappa_1 N\right)\right] s + HK_0\kappa_0 N = 0 \qquad (43)$$

where N represents the CMG nonlinear element (gimbal pivot friction). If $1/k_F$ and N are selected as the two parameters of interest in the limit cycle and stability investigation, one obtains three stability boundaries. The real root boundary is

$$N = 0 \quad , \tag{44}$$

and the boundary at infinity is

$$1/k_F = 0 \quad . \tag{45}$$

The imaginary root boundary may be written as

$$1/k_F = -I_v \Omega^2 [I_v I_{GE} \Omega^4 - (I_v \kappa_0 + HK_1 \kappa_1) \Omega^2 + HK_0 \kappa_0]/J \tag{46a}$$

$$N = I_v \Omega^4 [I_v \kappa_1 \Omega^2 - H(K_0 \kappa_1 + K_1 \kappa_0)]/J \tag{46b}$$

where the Jacobian J of the simultaneous equations obtained from the real and imaginary parts of equation (43) is

$$J = -\Omega^2 \left[I_v \kappa_1 \Omega^2 - H(K_0 \kappa_1 + K_1 \kappa_0)\right]^2 - [I_v I_G \Omega^4 - (I_v \kappa_0 + HK_1 \kappa_1) \Omega^2 + HK_0 \kappa_0]^2 \quad . \tag{46c}$$

For the general case, the $1/k_F$ - N parameter plane stability plot takes the form of Figure 30. The region of interest of this figure for limit cycle considerations is enlarged and plotted on Figure 31. Shown in Figure 10 is a sketch of the describing function relationship associated with the nonlinearity N of the Sperry model (Fig. 2), where

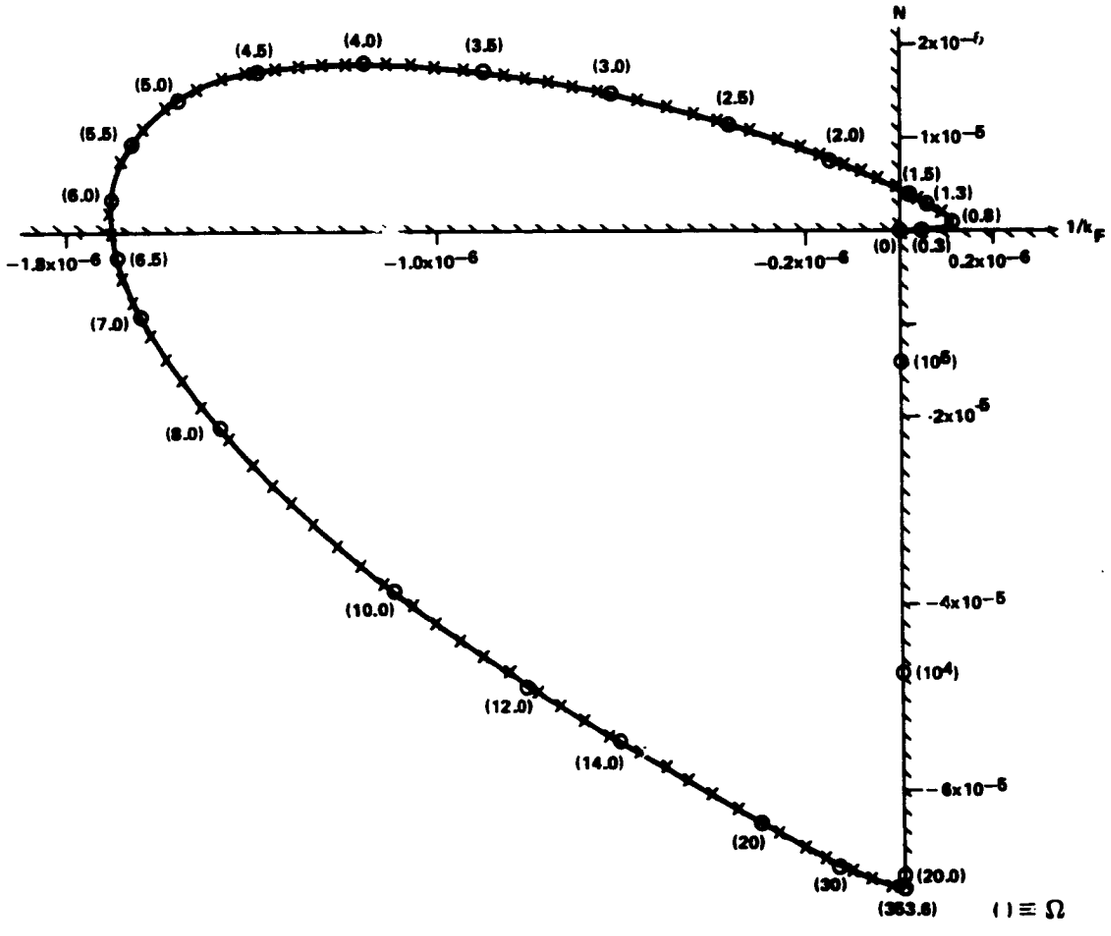

Figure 30. $1/k_F$ - N parameter plane — Sperry model.

$$N = 4M\sqrt{1 - (D/A)^2}\,/\pi A \quad , \quad A/D \geq 1 \quad . \tag{47}$$

If the nonlinear locus N (as a function of A) is reflected from the describing function graph onto the parameter plane, it is seen to be a vertical line rising from (and returning to) $1/k_F$ as A increases positively. Thus if $1/k_F > 1.16 \times 10^{-7}$ ($k_F < 8.62 \times 10^6$), no limit cycle can occur. If $1/k_F < 1.16 \times 10^{-7}$, then zero, two, or four limit cycles are predicted, depending on whether the peak value of $ND/M(= 2/\pi)$ intersects with none, one, or both of the portions of the complex root boundary. From Table 1 it is seen that the nominal value

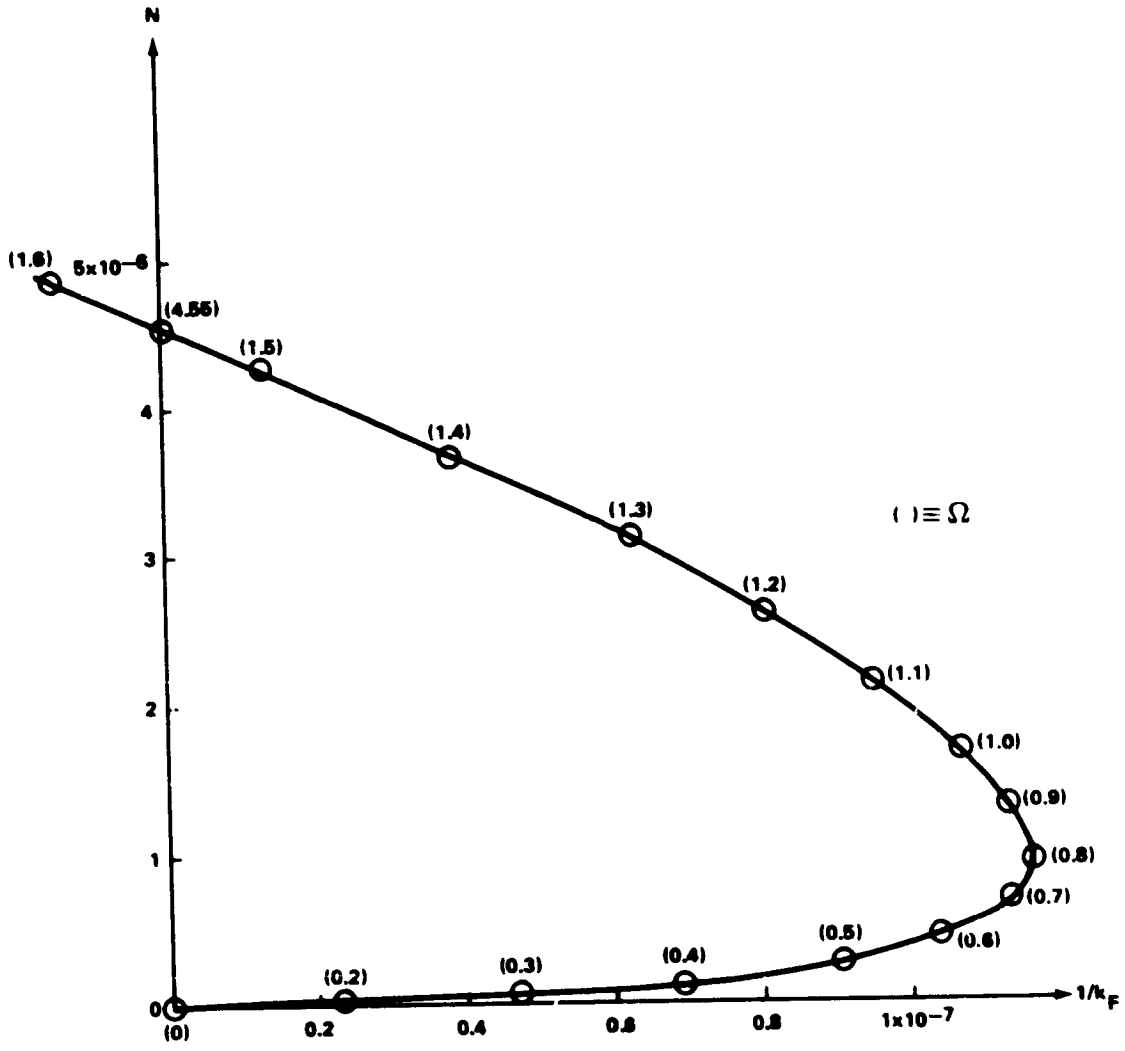

Figure 31. Limit cycle region of interest on parameter plane — Sperry model.

of k_F is 6600 ($1/k_F = 1.52 \times 10^{-4}$), indicating a wide margin of safety (for the numerical value chosen for the system parameters of this model) for precluding limit cycle operation. For example, if $M = 10D = 2.2 \times 10^{-3}$ and $1/k_F = 1 \times 10^{-7}$, then the lower value of N is 0.30×10^{-6} (with a corresponding value of $\Omega = 0.57$) and the upper value is 1.95×10^{-6} (and $\Omega \approx 1.06$). Since D is so small (with respect to unity), the two values of A corresponding to each value of N are [from equation (47)]

$$A \approx 4M/\pi N \quad , \quad 0 \qquad . \tag{48}$$

Thus two of the four indicated limit cycles have negligible amplitudes (A) and can be ignored. The other two significant amplitudes, the one corresponding to $N = 0.3 \times 10^{-6}$ being a stable limit cycle ($A^s = 9337$, $\Omega \approx 0.57$) and the other corresponding to $N = 1.95 \times 10^{-6}$ being unstable ($A^u = 1436$, $\Omega \approx 1.06$). These results were not confirmed by analogue simulation. It is felt by the author that they are sufficiently straightforward and do not warrant the effort.

ANALYSIS OF BENDIX MODEL NUMBER 2

An analysis of Bendix model number 2 was begun. Before it was completed, the momentum of opinion appeared to swing strongly in the direction of the "Dahl model" (see next analysis section). The author was swept away with this same enthusiasm and terminated analysis of Bendix Model No. 2.

ANALYSIS OF DAHL MODEL

The model chosen for the CMG and vehicle single-axis dynamics is shown in Figure 4. The nonlinear relationship (indicated by the symbol N) between gimbal friction torque T_F and gimbal angle δ is portrayed in Figure 5 and by equations (1) and (2). As in the above analyses, this analysis was based on using a describing function to represent the nonlinearity N. This in turn was based on the assumption of a sinusoidal input to the nonlinearity of amplitude A and frequency Ω.

Kuo described this nonlinearity by developing a describing function [11, 12]. Instead of using the straight line approximations conventionally used in the derivation of many describing functions, he used the actual curved lines precisely representing equations (1) and (2). Using the complex notation of N,

$$N = N_1 + iN_2 \quad , \tag{49}$$

Kuo obtained the following expressions:

$$N_1 \equiv \frac{\bar{B}_1}{A} \tag{50}$$

and

$$N_2 \equiv \frac{\bar{A}_1}{A} \tag{51}$$

where

$$\bar{A}_1 = -\frac{4T_{GFo}}{\pi} + \frac{1}{\pi A\gamma} \ln\left[\frac{(C_2 - A)(C_1 + A)}{(C_2 + A)(C_1 - A)}\right] \tag{52}$$

and

$$\bar{B}_1 = -\frac{2}{\gamma A} - \frac{C_2}{\gamma A\sqrt{C_2^2 - A^2}} + \frac{C_1}{\gamma A\sqrt{C_1^2 - A^2}} \quad , \tag{53}$$

where

$$C_1 = A - \frac{1}{\gamma(T^+_{GFi} - T_{GFo})} \tag{54}$$

and

$$C_2 = -A - \frac{1}{\gamma(T^-_{GFi} + T_{GFo})} \quad , \tag{55}$$

where

$$T^{+}_{GFi} = - T_{GFo} \left(- \frac{1}{a} + \sqrt{\frac{a^2 + 1}{a^2}} \right) \tag{56}$$

and

$$T^{-}_{GFi} = T_{GFo} \left(- \frac{1}{a} + \sqrt{\frac{a^2 + 1}{a^2}} \right) \quad , \tag{57}$$

where

$$a = 2\gamma A \, T_{GFo} \quad . \tag{58}$$

The author found that Kuo's equations can be simplified considerably by observing that $C_2 = - C_1$ and $T^{-}_{GFi} = - T^{+}_{GFi}$, leading to

$$\bar{A}_1 = \frac{1}{\pi} \left[- 4 T_{GFo} + \frac{1}{A\gamma} \ln \left(\frac{C + A}{C - A} \right)^2 \right] \tag{59}$$

and

$$\bar{B}_1 = \frac{2}{\gamma A} \left(\frac{C}{\sqrt{C^2 - A^2}} - 1 \right) \tag{60}$$

where $C = C_1$. Alternately these expressions may be rewritten as functions of the arguments a and T_{GFo}, leading to

$$\bar{A}_1 = \frac{2T_{GFo}}{\pi}\left[\frac{1}{a}\ln\left(a+\sqrt{a^2+1}\right)^2 - 2\right] \tag{61}$$

and

$$\bar{B}_1 = \frac{4T_{GFo}}{a}\left[\sqrt{\frac{a^2+a+1+(a+1)\sqrt{a^2+1}}{2\left(a+\sqrt{a^2+1}\right)}} - 1\right] . \tag{62}$$

Approximations for these curves may be obtained by deriving the asymptotes for N_2 versus N_1. The asymptote associated with small values of a ($a << 1$) is

$$N_1 \approx \gamma T_{GFo}^2 \tag{63}$$

and the asymptote associated with large values of a ($a >> 1$) is

$$N_2 \approx \frac{(4T_{GFo})^{2/3}\gamma^{1/3}}{\pi} N_1^{2/3} . \tag{64}$$

The latter expression is simplified if one plots the real (N_1) and imaginary (N_2) parts of the describing function on log-log paper:

$$\log N_2 = \log K + \frac{2}{3}\log N_1 \tag{65}$$

where

$$K = \frac{(4T_{GFo})^{2/3}\gamma^{1/3}}{\pi} . \tag{66}$$

Hence one obtains a straight line with a slope of 2/3 and a y-intercept of K for one asymptote and a straight line, parallel to the v-axis, for the other asymptote. The effect of variations in the gimbal bearing parameters T_{GFo} and γ may now be seen explicitly.

Let k_T be the factor by which T_{GFo} is increased (or decreased), i.e. the new value of T_{GFo} is k_T times as large as the former value. Also let k_γ be the factor by which γ is increased (or decreased). Then, examination of equations (63) and (64) shows the effect of altering the numerical values of T_{GFo} and γ is to multiply the former values of N_1 and N_2 (of the describing functions) by the quantity, $k_T^2 k_\gamma$.

Now, a general map of N_2 versus N_1 may be developed for use in this and future limit cycle investigations for this particular form of nonlinearity. It is universal in the sense that it permits one to choose any value of T_{GFo} and γ and see its effect on the N_2 versus N_1 map, such as by placing it on an N_1, N_2 parameter plane stability map to predict and analyze limit cycle existence and behavior.

A new parameter is defined:

$$\sigma \equiv \gamma T_{GFo}^2 \quad . \tag{67}$$

Now, a map of N_2/σ versus N_1/σ is simply obtained by plotting the two straight lines (asymptotes) of equations (63) and (64) on Figure 32.

Values of A may also be found from Figure 32 by again resorting to approximations. For the asymptote associated with relatively large values of a,

$$N_2 \approx \frac{4T_{GFo}}{\pi A} \tag{68}$$

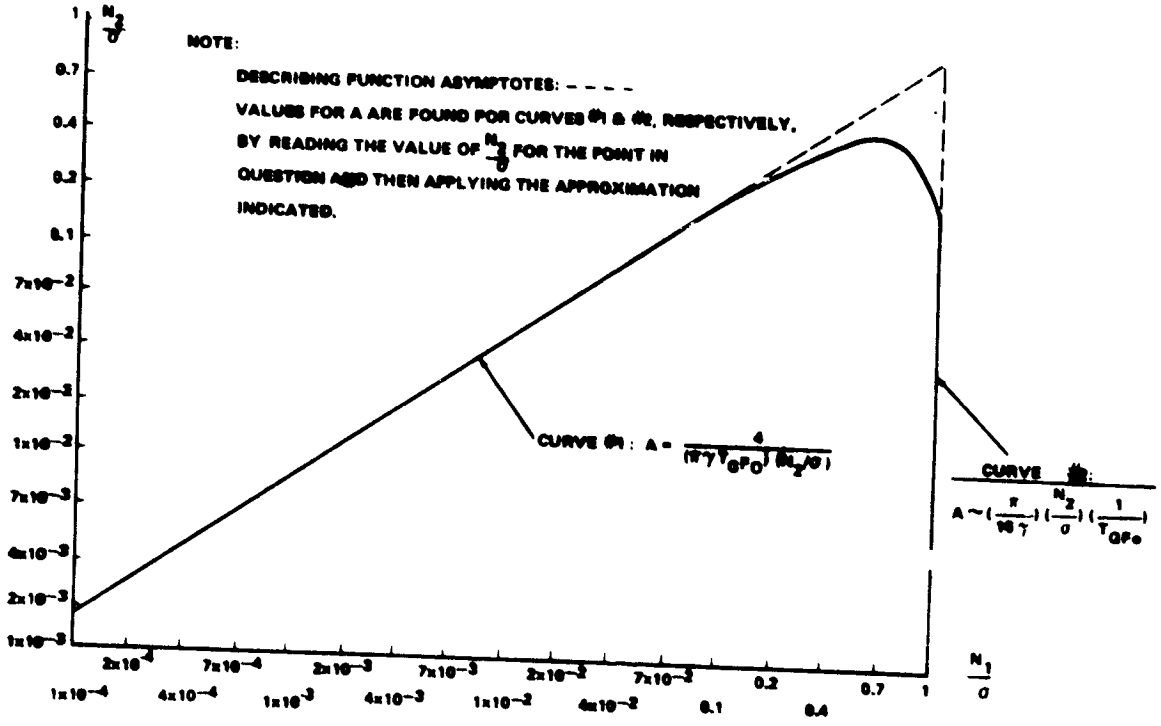

Figure 32. Normalized Dahl describing function locus.

which leads to an expression for A in terms of N_2/σ and parameters γ and T_{GFo}:

$$A \approx \frac{4}{(\pi\gamma T_{GFo})(N_2/\sigma)} \quad . \tag{69}$$

Thus for any location on the large a (slanting) asymptote (curve 1, Fig. 32), A may be determined for a given point by looking at the associated value of N_2/σ and using equation (69). For the range of numerical values used in the LST analysis, equation (69) has proven to be a fairly good approximation.

For the small a (vertical curve 2 on Fig. 32) asymptote, values of A are found by approximating equation (61) with a power series and truncating. Let the natural logarithm term, $(a + \sqrt{a^2 + 1})^2$, be approximated by the term,

$$\ell \quad 2a^2 + 2a + 1 \quad . \tag{70}$$

Then a power series expansion of $\ln \ell$ is

$$\ln \ell = 2\left[\frac{\ell - 1}{\ell + 1} + \frac{1}{3}\left(\frac{\ell - 1}{\ell + 1}\right)^3 + \ldots\right]$$

$$= \frac{2a(a+1)}{a^2 + a + 1} + \frac{2}{3}\left[\frac{a(a+1)}{a^2 + a + 1}\right]^3 + \ldots \quad . \tag{71}$$

Combining equation (71) with equations (61) and (51) leads to an approximation for A as a function of N_2/σ :

$$A \approx \left(\frac{\pi}{16\gamma}\right)\left(\frac{N_2}{\sigma}\right)\left(\frac{1}{T_{GFo}}\right) . \tag{72}$$

For LST numerical values, this turns out to be a poor, but barely acceptable, approximation. The problem in approximations arises, for LST numerical parameters, because a difference between two nearly identical numbers is required in equation (61).

Finally, equations (50), (51), (61), and (62) are used to determine the transition curve connecting the two asymptotes. The describing function plot of Figure 32 may now be used in conjunction with a stability contour, such as will be developed in the next section, on an N_1, N_2 parameter plane. If it is redrawn on a transparency it may be used with a stability map (as will be demonstrated on Figures 34 and 35) without redrawing it each time by displacing it in both the N_1 and N_2 direction by an amount equal to $k_T^2 k_\gamma$. (It has been redrawn on Figures 34 and 35 for the sake of clarity in this paper.)

As in the previous analyses, the possibility of limit cycle existence will be determined. When it is predicted that one exists, its characteristics will be determined.

The model shown in Figure 4 may be described in conventional control system form (closed loop transfer function) as

$$\frac{\theta}{T_c} = \frac{K_1}{I_v I_{GE} s^4 + I_v K_p s^3 + I_v (N + K_1) s^2 + K_I HA_I s + K_I HA_0} \quad . \qquad (73)$$

The characteristic equation associated with this model is

$$I_{GE} s^4 + \left(K_p + \frac{N_2}{\Omega} \right) s^3 + (K_I + N_1) s^2 + K_1 K_I s + K_0 K_I = 0 \qquad (74)$$

where

$$K_0 = \frac{HA_0}{I_v} \qquad (75)$$

and

$$K_1 = \frac{HA_1}{I_v} \quad . \qquad (76)$$

The system described by Figure 4 appears suitable for describing function analysis because it is low pass and the system parameters are assumed time invariant. A describing function N is used to represent the nonlinearity (herein assumed to be CMG gimbal friction). Recall that for a limit cycle to occur, it is required that all characteristic equation (74) roots have negative real parts except for one pair which must be purely imaginary roots. This condition is determined mathematically and, for ease of visualization, is portrayed graphically. In the latter case, two adjustable parameters are selected, N_1 and N_2. A correlation between these parameters and the roots of the characteristic equation is determined by mapping the stability contours from the complex s-plane onto the selected (N_1, N_2) parameter plane. For the system under consideration, only one such stability boundary exists and is easily found.

Analysis of equation (74) indicates the absence on the N_1, N_2 parameter plane of either a stability boundary associated with the real roots of the characteristic equation or the boundary at infinity.

The simultaneous solution of the nonlinear relation of equations (50) and (51) and the purely imaginary root boundary yields the condition for a limit cycle, assuming the indicated solution occurs adjacent to a stable region (true in this case). This condition is readily apparent on the parameter plane as the intersection (if one occurs) between the purely imaginary root boundary and the nonlinear locus of equations (50) and (51). From this point of intersection the frequency (Ω) and magnitude (A) of the indicated limit cycle(s) may be determined as functions of the characteristics of the nonlinearity and of the adjustable parameters. Further, the behavior of each limit cycle when a small perturbation is applied to its amplitude and, hence, the nature of limit cycle stability also is apparent on the parameter plane.

Turning to the characteristic equation (74) and setting $s = i\Omega$, one may obtain the real and imaginary parts of the equation:

$$-N_1\Omega^2 = -(K_0K_I - K_I\Omega^2 + I_{GE}\Omega^4) \tag{77}$$

and

$$-N_2\Omega = -(K_1K_I - K_p\Omega^2) \quad , \tag{78}$$

which yields the Jacobian

$$J = \Omega^3 > 0 \text{ if } \Omega > 0 \quad . \tag{79}$$

Solving equations (77) and (78) for the purely imaginary root boundary, one obtains

$$N_1 = \frac{I_{GE}\Omega^4 - K_I\Omega^2 + K_0K_I}{\Omega^2} \tag{80}$$

and

$$N_2 = \frac{-(K_p \Omega^2 - K_1 K_I)}{\Omega} \quad . \tag{81}$$

This boundary (cross-hatched curve) is sketched on Figure 33, the nature of the Jacobian indicating where the stable region lies. If the nonlinear locus of the describing function defined in equations (50), (51), (61), and (62) is also drawn on the same $N_1 - N_2$ plane, it is seen that several conditions can occur, depending on the numerical values selected for the system parameters. For a fixed set of values for I_{GE}, K_0, K_1, K_I, K_p, either no intersections (or predicted limit cycles) occur (Fig. 34a) or two intersections occur (Fig. 34b). In the latter case one limit cycle is stable (with indicated amplitude and frequency A^s and Ω^s, respectively) and one is unstable (A^u, Ω^u). In that case, if the amplitude (A) of the assumed simusoidal input to the nonlinearity is always less than A^u, the output of the nonlinearity will asymptotically approach zero. However if A ever exceeds the value A^u (such as by an initial condition), then A will approach A^s (and Ω will approach Ω^s). In the limiting case where the curves osculate but do not intersect, a single semistable (orbitally semistable) limit cycle is indicated. To interpret these phenomena physically, one may refer to Figure 4. The input to the nonlinearity is δ. For describing function analysis, it is assumed to be sinusoidal and of the form of equation (3), i.e.,

$$\delta = A \sin \Omega t \quad . \tag{82}$$

The output of the nonlinearity, T_f, is then assumed to be of the form

$$T_f \approx N\delta$$

$$= (N_1 + iN_2)\delta \tag{83}$$

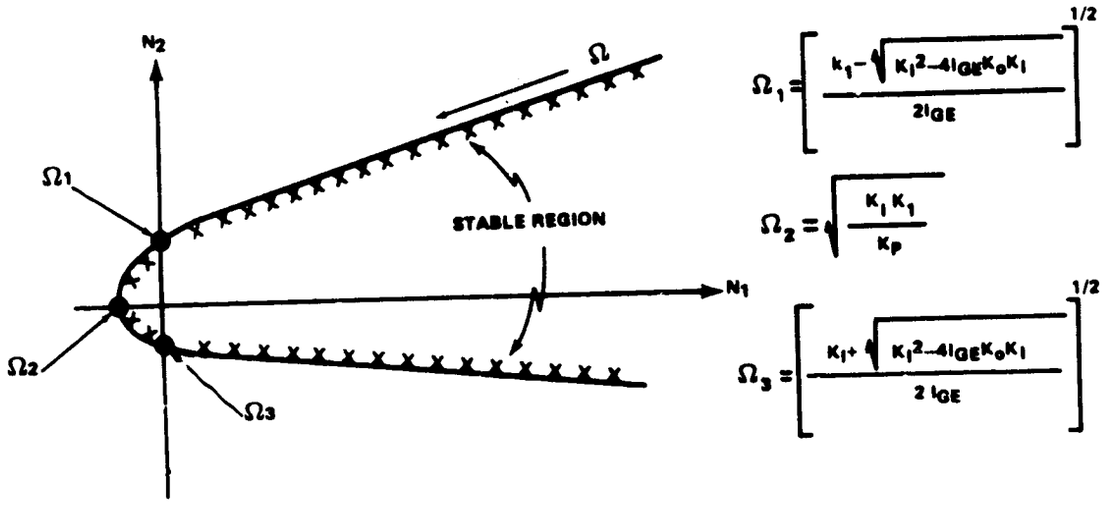

NOTE: $\Omega_1, \Omega_2, \Omega_3$ FOUND FROM EQUATIONS SHOWN.

Figure 33. $N_1 - N_2$ parameter plane — Dahl model.

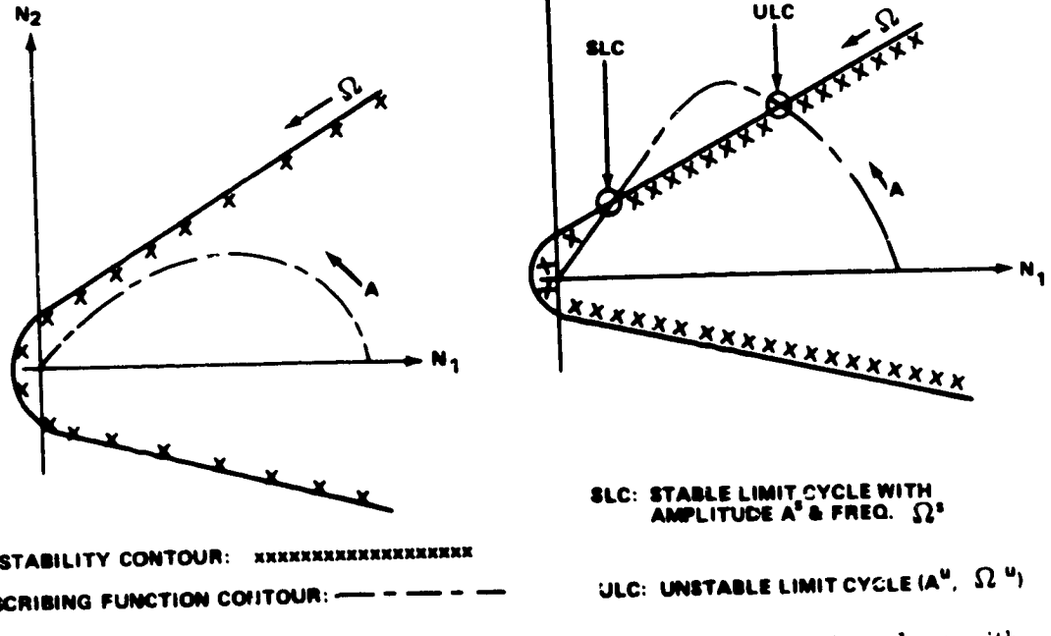

a. $N_1 - N_2$ parameter plane with no limit cycle.

b. $N_1 - N_2$ parameter plane with two limit cycles.

Figure 34. Dahl model.

$$= N_1 \delta + \frac{N_2}{\Omega} \dot{\delta}$$

$$= N_1 A \sin \Omega t + N_2 A \cos \Omega t$$

$$= A \sqrt{N_1^2 + N_2^2} \sin (\Omega t + \phi) \quad , \quad \phi = \tan^{-1} (N_2/N_1) \quad . \qquad (83)$$

(Concluded)

This is in the form of equation (4). Using equations (82) and (83) with the relations shown in Figure 4, one may now obtain the values of the other variables (e.g., $\dot{\theta}$ and θ) when $T_c \equiv 0$ and a limit cycle is predicted.

Typical numerical values of LST were altered slightly, because of the passage of time between analyses, and are shown in Table 3 (slightly different from Table 1). They are described in Reference 13.

TABLE 3. TYPICAL NUMERICAL VALUES FOR LST

Parameter	Numerical Value
A_0	2×10^4 (rad-s)$^{-1}$
A_1	3×10^3 (rad)$^{-1}$
H	271 Nms (200 ft-lb-s)
I_{GE}	5.012 Nms^2 (3.7 ft-lb-s^2)
I_v	1.354×10^5 Nms^2 (10^5 ft-lb-s^2)
K_I	1.354×10^4 Nm (10^4 ft-lb)
K_p	379 Nms (280 ft-lb-s)
T_{GFo}	C.271 Nm (0.2 ft-lb)
γ	1.477×10^5 (Nm rad)$^{-1}$ [2×10^5 (ft-lb rad)$^{-1}$]

The curve for the purely imaginary root boundary is found by substituting numerical values from Table 3 into equations (80) and (81). If Table 3 values for γ and T_{GFo} are used for the nonlinear locus representing the friction [equations (50), (51), (61), and (62)], it is seen that no intersections between the two curves will occur (Fig. 35). (This is the case portrayed in the sketch of Figure 34a.) Hence no limit cycles are predicted and stable operation is predicted.

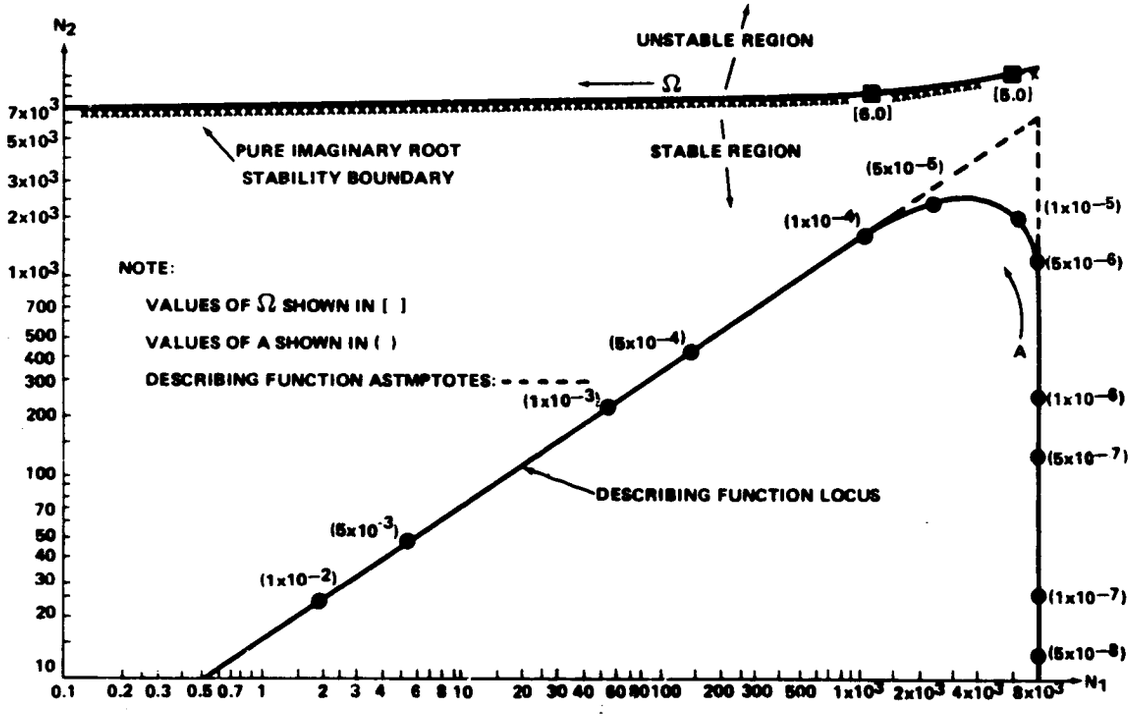

Figure 35. $N_1 - N_2$ parameter plane — Dahl model, $\gamma = 1.477 \times 10^5$.

If the asumptotes are also plotted on Figure 35, one sees that, if during the design evolution γ and/or T_{GFo} are increased, the case shown in the sketch of Figure 34b will occur. In that case two limit cycles are predicted, one stable and one unstable. One such example is shown in Figure 36, where γ is increased to a value of 1.477×10^6. The unstable limit cycle has a predicted amplitude of 1.0×10^{-6} rad and frequency of oscillations of 2.8 rad/s. The stable limit cycle amplitude is 2.1×10^{-5} rad with a frequency of oscillation of 5.2 rad/s. Practically, this means that if A has an initial value that is greater than 1.0×10^{-6} rad it will always converge to a value of 2.1×10^{-5} (the stable limit cycle). However, if the value of A is never permitted to exceed 1.0×10^{-6} rad (the unstable limit cycle), no limit cycle operation will occur and the system will be asymptotically stable.

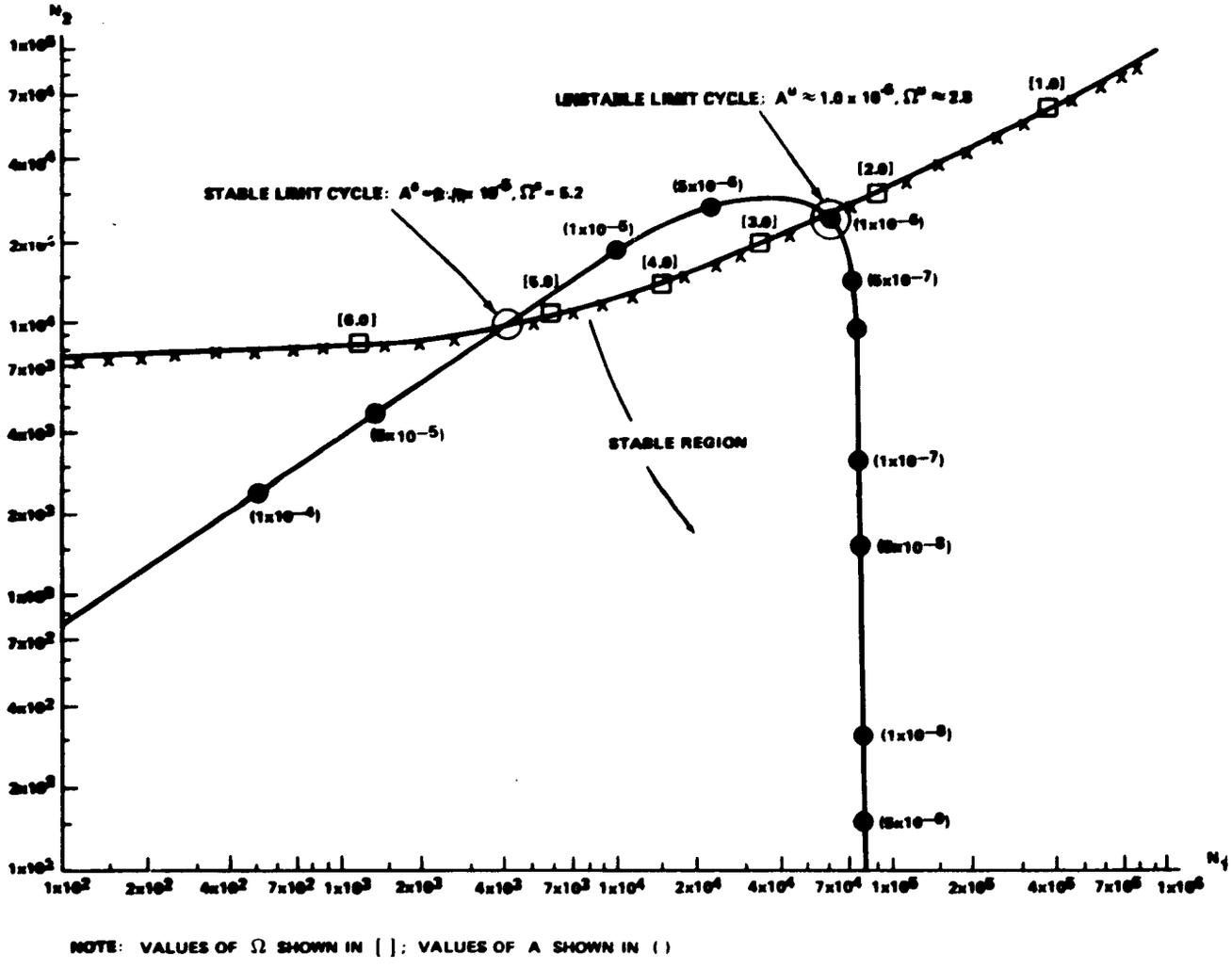

NOTE: VALUES OF Ω SHOWN IN [ ]; VALUES OF A SHOWN IN ( )

Figure 36. $N_1 - N_2$ parameter plane — Dahl model, $\gamma = 1.47 \times 10^6$.

The above predictions were confirmed with a simulation on an EAI 231R-V analogue computer, again through the efforts of Mr. P. H. Fisher. Figure 37 shows the stable limit cycle results, yielding measured values of 1.5×10^{-6} rad and 5.2 rad/s for the amplitude and frequency of oscillation of the gimbal angle (δ). Figure 38 shows the unstable limit cycle results, with values of 2×10^{-7} rad and 2.4 rad/s for gimbal angle amplitude and frequency, respectively. These values are sufficiently close to confirm the predicted value within the limits of describing functions analysis assumptions. A summary of the analytical predictions and simulation results is given in Table 4. Hence for the single nonlinearity considered, i.e., the output gimbal friction relation developed by Dahl, no limit cycle is predicted for presently estimated LST numerical parameters. However, if the design characteristics of the LST CMGs should allow numerical values of γ and/or T_{GFo} substantially larger than those indicated in Table 3, two limit cycles will occur, one stable, one unstable. A more detailed simulation effort has been described by G. S. Nurre.[5]

This analysis has considered neither the effect of multiple nonlinearities nor the effect of sampling (such as will be performed by an onboard digital computer). A sampled data analysis is now underway to consider the latter.

CONCLUSIONS

For numerical values considered to be representative of the LST and its CMGs, analysis indicates (and analogue simulation confirms) the absence of limit cycle bahavior due to the CMG output gimbal friction nonlinearity. Because of the present early stage of development of the LST, it is expected that the numerical values (and indeed mathematical characterization of CMG friction models) will change. Because of this, a wide spread of numerical values of actual variations in friction parameters has been examined. Further, a general technique of analysis of such system has been specified and used in great detail. This technique should be applicable to future alterations in the LST. As such, it provides a design tool for enhancing the efficiency of large scale computer simulation by predicting dynamic responses (thus aiding in the time-consuming debugging process) and in helping to select numerical values to be incorporated in the simulations. While the Dahl model has been widely accepted by those involved in CMG dynamics, the author respectfully points out that not too long ago the model termed herein as Bendix model number 1 was widely accepted (at least at MSFC).

5. G. S. Nurre, An Analysis of the Dahl Friction Model and its Effect on a CMG Gimbal Rate Controller, S&E-ASTR-A, Unnumbered report, MSFC, Oct. 18, 1973.

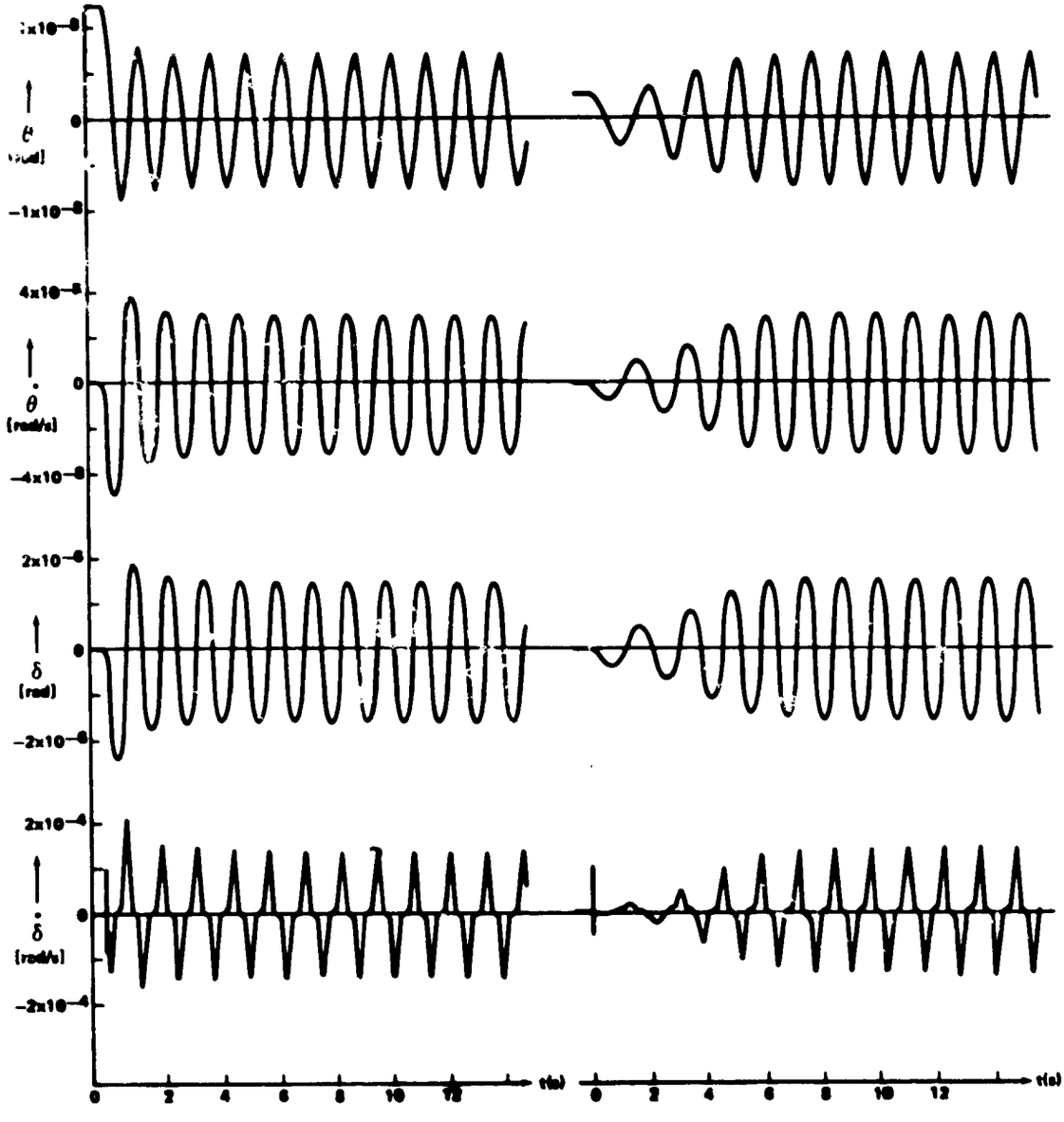

Figure 37. Dahl model simulation, $\gamma = 1.477 \times 10^6$.

The analysis of Bendix model number 1, in particular, is quite detailed, perhaps to the point of inciting boredom. However, not only is the general analysis technique presented but also a study of the effect of parameter variations is presented. Also, from an academic viewpoint, it is interesting (to some) to see actual examples of such usually obscure limit cycle behavior as orbitally semistable limit cycles.

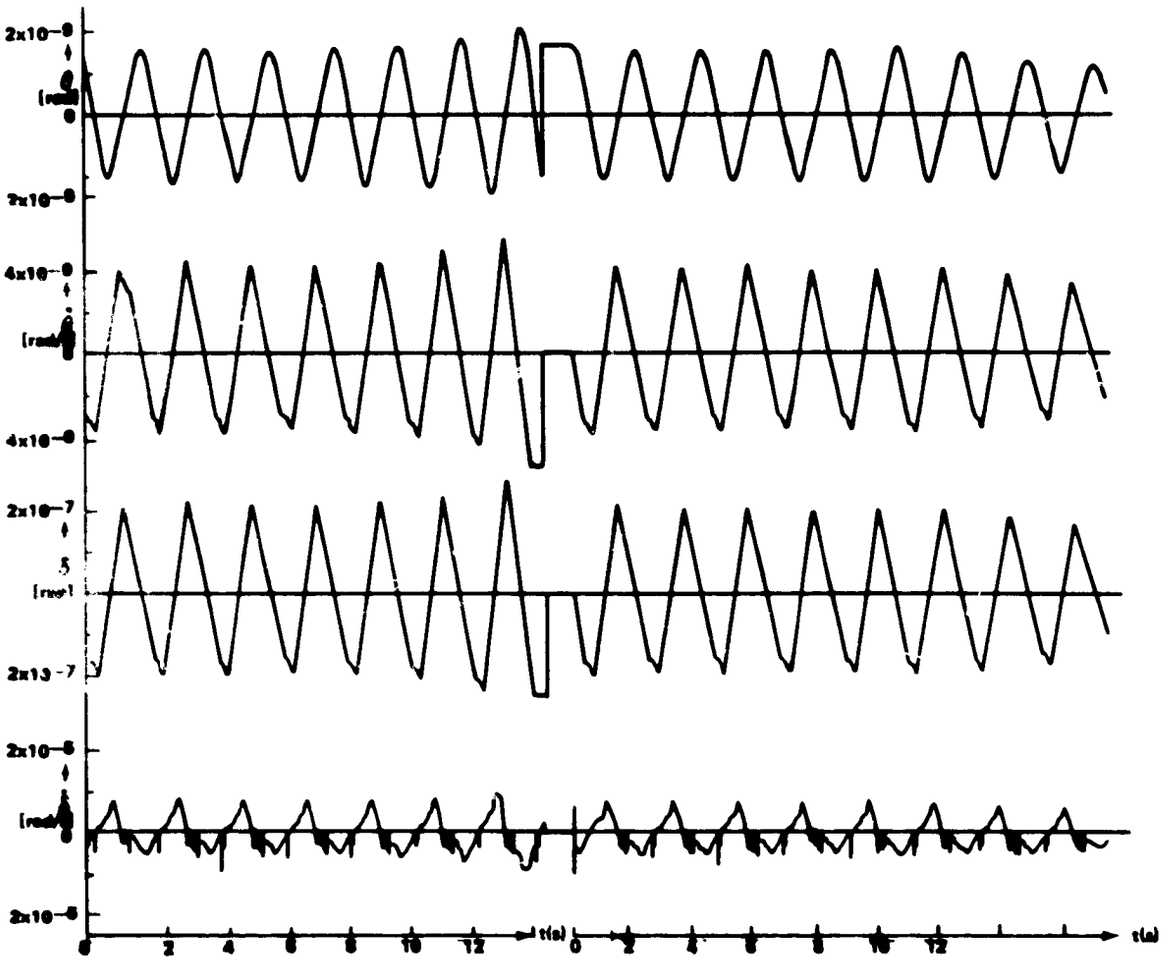

Figure 38. Dahl model simulation, $\gamma = 1.477 \times 10^6$.

TABLE 4. SUMMARY OF DAHL MODEL RESULTS

γ (Nm rad)$^{-1}$ [(ft-lb rad)$^{-1}$]	Limit Cycle	Analytical Predictions		Simulation Results			
		A (rad)	Ω (rad/s)	A (rad)	Ω (rad/s)	θ (rad)	$\dot{\theta}$ (rad/s)
$1.477\ (2 \times 10^5)$	No						
$1.477\ (2 \times 10^6)$	Unstable	1.0×10^{-6}	2.8	2.0×10^{-7}	2.4	1.6×10^{-9}	4×10^{-7}
$1.477\ (2 \times 10^6)$	Stable	2.1×10^{-6}	5.2	1.5×10^{-6}	5.2	7.5×10^{-7}	3×10^{-6}

REFERENCES

1. Seltzer, S.M.: Analysis of a Control System Containing Two Nonlinearities. Int. J. Control, 1970, vol. 10, no. 2, pp. 1058-1064.

2. Connell, G.M.: A Method of Earth Pointing Attitude Control for Elliptic Orbits. AIAA Journal, vol. 10, no. 3, Mar. 1972, pp. 258-263.

3. Schiehlen, W.: Comment on A Method of Earth-Pointing Attitude Control for Elliptic Orbits. AIAA Journal, vol. 11, no. 1, Jan. 1973.

4. Rybak, S.C.: Research and Applications Module (RAM) Phase B Study: Free Flyer GN&C Trade Study Report. RAM-B-GNC-407, Bendix Corp., Denver Facility, Oct. 29, 1971.

5. Rybak, S.C.: High Accuracy Stabilization and Control. Technical Report MT-2383, Bendix Corp., Denver Facility, Dec. 14, 1971.

6. Frieder, M.: A Note on CMG Characteristics and Spacecraft Limit Cycling. Engineering File MT-15, Bendix Corp., Teterboro, N.J., Apr. 19, 1972.

7. Andronow and Chaikin: Theory of Oscillations. Princeton University Press, N.J., 1949, pp. 203-208.

8. Ogata K.: Modern Control Engineering. Prentice-Hall, N.J., 1970, pp. 585-587.

9. Gelb and Vander Velde: Multiple-Input Describing Functions and Non-Linear Systems Design. McGraw Hill, N.Y., 1968.

10. Siljak, D.D.: Nonlinear Systems. Wiley, N.Y., 1969, pp. 152-171, 177-186.

11. Kuo, B.C.; Singh, G.; Yackel, R.A.: Modeling of the LST System with the CMG Nonlinear Friction. Report II-73, NASA Contract NAS8-29853, DCN-1-2-40-23018, Systems Research Lab., Champaign, Ill., Sept. 1, 1973.

12. Kuo, B.C.; Singh, G.; Yackel, R.A.: Continuous and Discrete Describing Function Analysis of the LST System. Report No. III-73, NASA Contract NAS8-29853, Systems Research Lab., Champaign, Ill., Nov. 1, 1973.

REFERENCES (Concluded)

13. **Liden, S.P.: Precision CMG Control for High-Accuracy Pointing.** AIAA Paper No. 73-871, Guidance and Control Conference, Key Biscayne, Fla., Aug. 20-22, 1973.

APPROVAL

NASA TM X-64833

CMG-INDUCED LST DYNAMICS

By Sherman M. Seltzer

The information in this report has been reviewed for security classification. Review of any information concerning Department of Defense or Atomic Energy Commission programs has been made by the MSFC Security Classification Officer. This report, in its entirety, has been determined to be unclassified.

This document has also been reviewed and approved for technical accuracy.

F. B. Moore
Director, Astrionics Laboratory

☆ U.S. GOVERNMENT PRINTING OFFICE 1974 - 748 297 / 150 REGION NO. 4